AIDS RESEARCH AND HUMAN RETROVIRUSES
Volume 28, Number 8, 2012

DOI: 10.1089/aid.2011.0180

The Hematopoietic Cell-Specific Rho GTPase Inhibitor ARHGDIB/D4GDI Limits HIV Type 1 Replication

Tadashi Watanabe,[1] Emiko Urano,[2] Kosuke Miyauchi,[2] Reiko Ichikawa,[2] Makiko Hamatake,[2] Naoko Misawa,[1] Kei Sato,[1] Hirotaka Ebina,[1] Yoshio Koyanagi,[1] Jun Komano[2]

Abstract

Rho GTPases are able to influence the replication of human immunodeficiency virus type 1 (HIV-1). However, little is known about the regulation of HIV-1 replication by guanine nucleotide dissociation inhibitors (GDIs), one of the three major regulators of the Rho GTPase activation cycle. From a T cell-based cDNA library screening, ARHGDIB/RhoGDIβ, a hematopoietic lineage-specific GDI family protein, was identified as a negative regulator of HIV-1 replication. Up-regulation of ARHGDIB attenuated the replication of HIV-1 in multiple T cell lines. The results showed that (1) a significant portion of RhoA and Rac1, but not Cdc42, exists in the GTP-bound active form under steady-state conditions, (2) ectopic ARHGDIB expression reduced the F-actin content and the active forms of both RhoA and Rac1, and (3) HIV-1 infection was attenuated by either ectopic expression of ARHGDIB or inhibition of the RhoA signal cascade at the HIV-1 Env-dependent early phase of the viral life cycle. This is in good agreement with the previous finding that RhoA and Rac1 promote HIV-1 entry by increasing the efficiency of receptor clustering and virus-cell membrane fusion. In conclusion, the ARHGDIB is a lymphoid-specific intrinsic negative regulator of HIV-1 replication that acts by simultaneously inhibiting RhoA and Rac1 functions.

Introduction

The human immunodeficiency virus type I (HIV-1) is the causative agent of acquired immunodeficiency syndrome (AIDS). The clinical success of Maraviroc, an antiretroviral drug that targets the host cell protein CCR5, demonstrates the importance of understanding host-HIV-1 interaction as this information will provide the basis for the development of the next generation of antiretroviral drugs. HIV-1 replicates primarily in CD4-positive T cells. However, aside from the viral receptors CD4 and CCR5, few lymphoid cell-specific regulators of HIV-1 replication have been identified. This is partly due to the use of nonlymphoid cells to screen for cellular factors that regulate HIV-1 replication, as these cells support the efficient transduction of genetic materials. Therefore, T cell-based cDNA library screening has some advantages, as discussed later.

Members of the Rho GTPase family, including RhoA, Rac1, and Cdc42, have been reported to regulate the replication of HIV-1 at various stages of the viral life cycle, including viral entry, transcription, and viral release.[1–7] Although these proteins are widely expressed, genome-wide screens for proteins that regulate HIV-1 replication using siRNA or shRNA libraries have failed to identify Rho GTPases.[8–10] This may suggest that Rho GTPases are not potent regulators of HIV-1 replication and are therefore difficult to detect unless the viral replication assay is employed, since multiple replication cycles augment the biological effects of Rho GTPases.

There are three major regulators of the activation cycle of Rho GTPases: guanine nucleotide exchange factors (GEFs), GTPase-activating proteins (GAPs), and guanine nucleotide dissociation inhibitors (GDIs or ARHGDIs). RhoGEFs promote the exchange of GDP for GTP, RhoGAPs accelerate GTP hydrolysis, and ARHGDIs stabilize the GDI-bound form of Rho GTPases and also mask the lipid moiety of Rho GTPases, thereby sequestering Rho GTPases at the plasma membrane.[11–14] Some RhoGAPs and RhoGEFs have been known to regulate HIV-1 replication.[6,9,10,15–18] Positive regulators of Rho GTPases, such as RhoGEFs, were identified in the genome-wide screens, although these studies yielded varying results. In this sense, the upstream regulators of Rho GTPases may more potently influence HIV-1 replication than Rho GTPases themselves when expression levels are dysregulated. ARHGDIs have yet to be identified as regulators of HIV-1 replication.

[1]Laboratory of Viral Pathogenesis, Institute for Virus Research, Kyoto University, Kyoto, Japan.
[2]AIDS Research Center, National Institute of Infectious Diseases, Tokyo, Japan.

Previously, we established a genetic screening system using a T cell-derived cDNA library to isolate cellular factors that render cells resistant to HIV-1 replication.[19,20] This system is unique in that the screen is based on MT-4 cells, a human CD4-positive T cell line, which were exposed to replication-competent HIV-1. Using this system, the carboxy-terminal domains of Brd4 and SEC14L1a were found to be negative regulators of HIV-1 replication.[19,20] Importantly, these factors were not found in previous genetic screens, suggesting that our system complements other genome-wide analyses. In this study, we describe a lymphoid-specific RhoGDI that negatively regulates HIV-1 replication through attenuation of both RhoA and Rac1 functions.

Materials and Methods

Cells

Cells were maintained in RPMI 1640 medium (Sigma, St. Louis, MO) supplemented with 10% fetal bovine serum (FBS; Japan Bioserum, Tokyo, Japan or Thermo Fisher Scientific Inc., Waltham, MA), 50–100 U/ml penicillin, and 50–100 μg/ml streptomycin (Invitrogen, Tokyo, Japan), and then incubated at 37°C in a humidified 5% CO_2 atmosphere. The selection of cDNA library-transduced cells was described previously.[20] To select puromycin-resistant cells after infection with pQc- or pSM2c-based murine leukemia virus (MLV) vector, 1 μg/ml puromycin (Sigma) was added to the culture medium.

Plasmids

The plasmid vectors pCMMP, pMDgag-pol, pSV-tat, phRL/CMV, and pVSV-G were described previously.[21] The shRNA expression vectors pSM2c and pSM2/ARHGDIB (RHS1764-9680880) were purchased from Thermo Fisher Scientific (Open Biosystems Products, Huntsville, AL). The pQcXIP was obtained from Clontech (BD Biosciences Clontech, Palo Alto, CA). pGEX-Rhotekin-RBD and pGEX-4T-PAK2-RBD were kindly provided by S. Narumiya, Kyoto University.[3,22] To construct pLTR-hRL, the HIV-1_{HXB2} long terminal repeat (LTR) was amplified by PCR using the following primers: 5′-GGA TCC TGG AAG GGC TAA TTC ACT CC-3′ and 5′-GCT AGC TGC AGC TGC TAG AGA TTT TCC ACA CTG-3′. The *Bgl*II-*Nhe*I fragment of the PCR product was cloned into the corresponding restriction sites of phRL/CMV, generating pLTR-hRL. The LTR-Luc plasmid was described previously.[23] To construct pCMV-Tat-FLAG, HIV-1_{NL4-3} *tat* was amplified from cDNA prepared from HIV-1-infected MT-4 cells by RT-PCR using the following primers: 5′-ATG GAG CCA GTA GAT CCT AGA CTA GAG CCC T-3′ and 5′-TTC CTT CGG GCC TGT CGG GT-3′. The PCR product was cloned into the *Eco*RV sites of pcDNA3.1 Zeo(+) bearing FLAG-tags at the *Not*I-*Xho*I site (Invitrogen). The pCMV-Luc plasmid was a generous gift from Dr. Hijikata (Kyoto University).

Flow cytometry

Cells were incubated with anti-CD4, anti-CD8, or anti-CXCR4 monoclonal antibodies conjugated to R-phycoerythrin (PE; BD Pharmingen, San Diego, CA) for 30 min at 4°C. Cells were washed once with phosphate-buffered saline (PBS) supplemented with 1% FBS and analyzed by FACS Calibur (Beckton Dickinson, San Jose, CA).

Phalloidin staining of F-actin

Phalloidin staining of F-actin was performed as described previously.[24] In brief, cells were fixed, permeabilized by cytofix/cytoperm (BD Bioscience) for 20 min on ice, washed, and stained with Alexa Fluor 647-phalloidin (Invitrogen) for 30 min at 4°C. Samples were kept on ice until analysis by FACS Calibur or Canto II (Beckton Dickinson, San Jose, CA). The flow cytometric data were analyzed using FlowJo version 9.3 (Tree-star Inc., Ashland, OR).

Viruses

The retroviral vector pCMMP, carrying the MT-4 cDNA library and a green fluorescent protein (GFP) expression cassette, was obtained from Takara (Takara, Otsu, Japan). Full-length ARHGDIB was cloned from a lymph node cDNA library (Takara) by RT-PCR using the primers 5′-GCA CCG GTC TCG AGC CAC CAT GAC TGA AAA AGC CCC AGA GC-3′ and 5′-CCA ATT GGA TCC TCA TTC TGT CCA CTC CTT CTT AAT CG-3′, and cloned into the pCMMP vector. The MLV vectors were produced by tripartite transfection of pMDgag-pol, pVSV-G, and either pCMMP, pQc, or pSM2c retroviral vector. Cells were infected with the MLV vectors as described previously.[21] The production of replication-competent HIV-1_{HXB2} and the measurement of replication kinetics were performed as described previously.[21]

Western blotting

Western blotting was performed according to techniques described previously.[25] The following monoclonal antibodies were used: anti-RhoA (C-11; Santa Cruz Biotechnology, Santa Cruz, CA), anti-Rac1 (23A8; Millipore, Japan), anti-Cdc42 (B-8; Santa Cruz Biotechnology), anti-ARHGDIB (A01; Abnoba, Taiwan), anti-$p24^{CA}$ (183-H12-5C; NIH AIDS Research and Reference Reagent Program), anti-actin (clone C4; Millipore), and anti-tubulin (DM1A; Sigma). Densitometric analysis was performed using ImageJ ver. 1.43 software (obtained from http://rsbweb.nih.gov/ij/index.html).

Active Rho GTPase capture assay

We adopted a protocol described previously.[3,22] In brief, the glutathione *S*-transferase (GST) fused to the Rho GTPase binding domain (RBD) of Rhotekin and GST fused to the RBD of PAK2 were expressed in *E. coli* and purified by incubating the cell lysates with glutathione-Sepharose 4B beads (GE Healthcare Bio-Sciences, Piscataway, NJ) for 3 h at 4°C. The beads were washed three times with ice-cold Rho buffer (25 mM HEPES, pH 7.5, 150 mM NaCl, 10 mM $MgCl_2$, 1 mM EDTA, 10% Glycerol). Finally, the beads were washed with ice-cold Rho buffer supplemented with 1% NP-40 and protease inhibitor cocktail tablets (Complete, Roche Diagnostics GmbH, Mannheim, Germany). Cells were incubated in ice-cold Rho buffer for 15 min on ice, and the cell lysates were clarified by centrifugation at 18,000 × *g* at 4°C for 20 min. A fraction of the cleared cell lysates was incubated at 37°C for 30 min as a negative control or coincubated with GTPγS (0.1 mM, Sigma) for 30 min at 30°C as a positive control. These preparations were incubated with the above beads at 4°C for 1 h. The beads were washed three times with Rho buffer containing 1% NP-40 and subjected to SDS-PAGE followed by Western blotting. The bead-bound GTPases were detected

using a monoclonal antibody against RhoA, Rac1, or Cdc42, as appropriate.

Single-round infection assay

Single-round virus infection and luciferase assays were performed as described previously.[21,26] In brief, cells were exposed to viral preparations containing 1–10 ng of $p24^{CA}$. Luciferase activities were measured at 2–3 days postinfection with the Picagene luciferase assay kit (Toyo Ink, Tokyo, Japan) or Steady-Glo kit (Promega, Tokyo, Japan) according to the manufacturer's protocols. For the inhibition of Rho-kinase (ROCK), cells were pretreated with 12.5 μM Y27632 (Nakalai tesque, Kyoto, Japan) for 1 h and incubated with the viral preparation in the presence of 12.5 μM Y27632 for 4 h. Cells were washed with tissue culture medium and cultivated for 2 days. Light emission was detected with a 1420 ARVOSX multilabel counter (Perkin Elmer, Wellesley, MA) or a Veritas luminometer (Promega).

Single-round production assay

Five million PM1/control or PM1/ARHGDIB cells were resuspended in 250 μl of STBS (25 mM Tris-Cl, pH 7.4, 137 mM NaCl, 5 mM KCl, 0.6 mM Na_2HPO_4, 0.7 mM $CaCl_2$, and 0.5 mM $MgCl_2$), including 10 μg of pHXB2 proviral plasmid DNA. Cells were mixed with 250 μl of STBS containing 1 mg/ml of DEAE-Dextran and incubated for 30 min at room temperature (RT). The cells were then incubated with STBS containing 10% DMSO for 2 min at RT and washed with 1 ml HBSS (Invitrogen). Transfected cells were cultured in RPMI medium containing 10% FBS and 1 μM efavirenz. After 2 days in culture, viruses in the culture supernatant were pelleted by ultracentrifugation on a 20% sucrose cushion. Cells and viruses were lysed with radioimmunoprecipitation assay (RIPA) lysis buffer (0.05 M Tris-HCl, 0.15 M NaCl, 1% Triton X-100, 0.1% sodium dodecyl sulfate, and 1% sodium deoxycholate) and electrophoresed in a 10% polyacrylamide gel for SDS–PAGE. Proteins were then transferred to a PVDF membrane, and $p24^{CA}$ was detected by immunoblot analysis using an anti-$p24^{CA}$ antibody.

Reporter expression assay

The luciferase-expressing reporter plasmids were transfected into PM1 cells according to the DEAE-Dextran method as described above. For transfection, either 1 μg of pCMV-Luc, 10 μg of pLTR-Luc, 0.5 μg of phRL/CMV, or 1 μg of pLTR-hRL was used. The pLTR-Luc and pLTR-hRL were co-transfected with 5 μg of pCMV-tat-FLAG and 1 μg of pSVtat, respectively. Firefly luciferase activity was measured as described above. Renilla luciferase activity was also measured as described above, except that the Renilla Luciferase Assay System (Promega) was used in place of the Steady-Glo kit. The data were analyzed using a two-tailed Student's *t*-test.

Results

Identification of RhoGDIβ/ARHGDIB as a negative regulator of HIV-1 replication

A pool of MT-4 cells constitutively expressing a cDNA library transduced with an MLV-based retroviral vector was used to screen for possible regulators of HIV-1 replication. The MLV vector carried an expression cassette for GFP and inserts from a cDNA library derived from MT-4 cells (Fig. 1A). The cDNA-transduced cells were enriched with a cell sorter using GFP as a marker. These cells were then infected with CXCR4-using (X4) $HIV\text{-}1_{HXB2}$. MT-4 cells have been shown to support efficient HIV-1 production and rapidly undergo cell death after infection. The surviving MT-4 cells were propagated and genomic DNA was isolated to identify the inserted cDNA, as described previously.[19] These genes were considered potential negative regulators of HIV-1 replication. A cDNA clone encoding ARHGDIB (RhoGDIβ/LyGDI/D4GDI; gene ID 397) was recovered from the MT-4 cDNA library (1/94 independent clones, 1.1%).

Full-length ARHGDIB cDNA was cloned into the MLV vector pQcXIP, and a T cell line expressing ARHGDIB at levels higher than endogenous levels was established. To verify the HIV-1-resistant phenotype of ARHGDIB, the rate of HIV-1 replication was assessed in MT-4 cells subjected to ectopic ARHGDIB expression. In these cells, ARHGDIB levels were increased by approximately 4.9-fold compared with control cells, while the cell surface expression of CD4 and CXCR4 was not significantly affected in MT-4 cells (Fig. 1B). Even the modest up-regulation of ARHGDIB delayed HIV-1 replication kinetics (Fig. 1B). Suppression of HIV-1 replication was independently reproduced in MT-4 cells, even when a different retroviral vector, pCMMP, was used to transduce ARHGDIB (data not shown). In addition, neither the rate of cell proliferation nor cell morphology was affected by stable ectopic expression of ARHGDIB over at least 6 months in culture (data not shown). Delayed HIV-1 replication in cells ectopically overexpressing ARHGDIB was also observed in PM1 (Fig. 1C), M8166 (Fig. 1D), and Jurkat cells (Fig. 1E), in which ARHGDIB levels were increased by 2.1-, 1.9-, and 1.5-fold, respectively, compared with control levels. Similar data were also obtained in SUP-T1 cells (data not shown). The delayed HIV-1 replication in cells ectopically expressing ARHGDIB was reproduced in 10 independent experiments ($p < 0.01$, two-sided binomial test), strongly suggesting that ARHGDIB attenuates the replication of HIV-1. These results indicate that enhanced expression of ARHGDIB renders cells resistant to HIV-1 replication. Consistent with these data, the shRNA-mediated down-regulation of ARHGDIB accelerated the replication of HIV-1 in MT-4 cells (Fig. 1F). These data support the idea that ARHGDIB is a negative regulator of HIV-1 replication.

The RhoGDI family has three members, α, β, and γ, which correspond to ARHGDI A, B, and C, respectively.[11] RhoGDI family members are known to regulate Rho GTPases, including RhoA, Rac1, and Cdc42, although some nonredundant functions of RhoGDIs have been reported.[27] ARHGDIB/RhoGDIβ is primarily expressed in cells of a hematopoietic lineage. Given that Rho GTPases are known to be positive regulators of HIV-1 replication and that ARHGDIB is a negative regulator of Rho GTPases in hematopoietic cells, the function of ARHGDIB was investigated in further detail.

Molecular mediators in the inhibition of HIV-1 replication by ARHGDIB

Under *in vitro* culture conditions, T cell lines show a constitutively activated cell phenotype, and Rho GTPases, including RhoA, Racl, and Cdc42, have been implicated in T cell

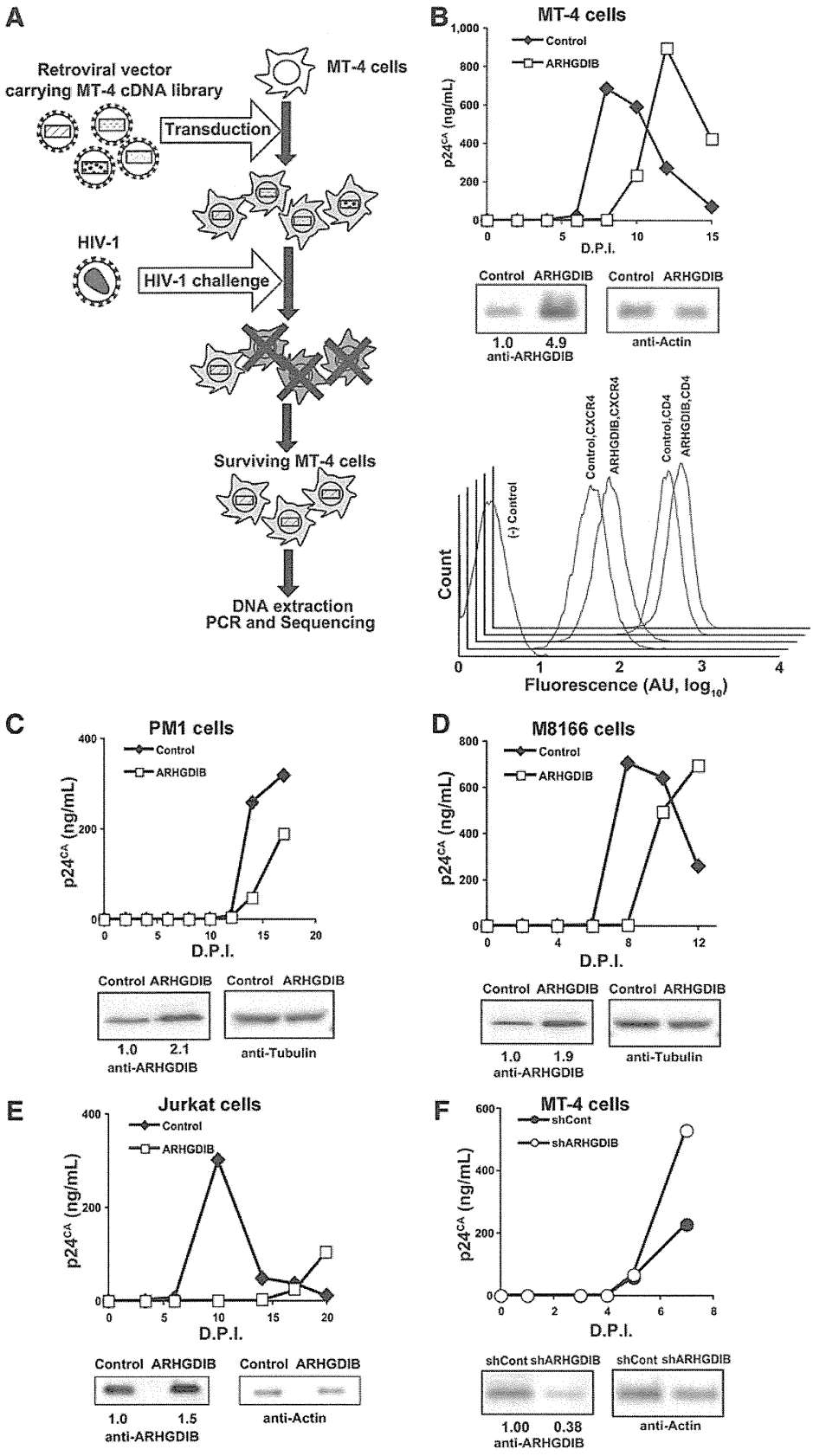

FIG. 1. Isolation and characterization of ARHGDIB as a negative regulator of HIV-1 replication. **(A)** The screening strategy used to isolate genes that render MT-4 cells resistant to HIV-1 replication. **(B–E)** Ectopic expression of ARHGDIB (open rectangles) in MT-4 **(B)**, PM1 **(C)**, M8166 **(D)**, and Jurkat **(E)** cells delayed the replication kinetics of HIV-1. Representative data from five, two, and two independent experiments for MT-4, M8166, and Jurkat cells are shown, respectively. The control counterpart is shown as filled diamonds. **(B)** The flow cytometric profiles of MT-4 cell surface CD4 and CXCR4 are shown. MT-4/ARHGDIB cells stained for CD8 were used as a negative control. **(F)** Down-regulation of ARHGDIB (open circles) in MT-4 cells accelerated the replication of HIV-1. The control counterpart is shown as filled circles. **(B–F)** Expression levels of ARHGDIB and an internal control, either actin or tubulin, were assessed by Western blot analysis. The magnitude of ARHGDIB up- or down-regulation was determined by densitometry and is indicated below each image. AU, arbitrary unit; D.P.I., days postinfection.

activation.[28–30] These Rho GTPases are expressed in various T cell lines, including MT-4, PM1, and M8166 cells, as confirmed by RT-PCR analysis (data not shown). It seemed likely that augmented ARHGDIB expression affected HIV-1 replication by modulating the activity of these Rho GTPases. Thus, the activation status of RhoA, Rac1, and Cdc42 was determined in relation to the enhanced expression of ARHGDIB.

Rho GTPases are intrinsically inefficient hydrolyzing enzymes that quickly cycle between GTP-bound active and GDP-bound inactive forms. If ARHGDIB attenuates HIV-1 replication by inhibiting Rho GTPase activities, some fraction of Rho GTPases would exist in a GTP-bound active form under steady-state tissue culture conditions, and this population should be decreased in cells ectopically expressing ARHGDIB. Using an active Rho GTPase capture assay, the levels of active Rho GTPases in control and ARHGDIB-expressing cells were measured (Fig. 2A). In this assay, GTP-bound Rho GTPase is captured by glutathione-Sepharose beads conjugated to GST fused to the Rho binding domain of Rhotekin or PAK2. The active forms of both RhoA and Rac1, but very little Cdc42, were detected in PM1 cells under steady-state tissue culture conditions (Fig. 2B–D). Activation levels under the steady-state conditions were estimated by comparing the captured Rho GTPase signals with the maximal activation levels, which were established by converting all Rho GTPases to an active form by GTPγS before the pull-down procedure. The activated fractions of Rac1, RhoA, and Cdc42 were 34.2%, 23.2%, and 0.0%, respectively (Fig. 2B–D). Importantly, ectopic expression of ARHGDIB reduced the activated fractions of RhoA and Rac1 to 4.1% and 3.6%, respectively (Fig. 2B and C). Similar observations were made for MT-4 and SUP-T1 cells (data not shown).

These observations clearly indicated that ARHGDIB attenuates RhoA and Rac1 activity simultaneously in these T cell lines and suggested that RhoA and Rac1 are the primary targets of ectopically expressed ARHGDIB. Note that RhoA and Rac1 levels were increased by 1.4- and 1.3-fold, respectively, in cells ectopically expressing ARHGDIB, according to the densitometric analysis (Fig. 2B and C). This is due to the ARHGDIB-mediated stabilization of Rho GTPases, as

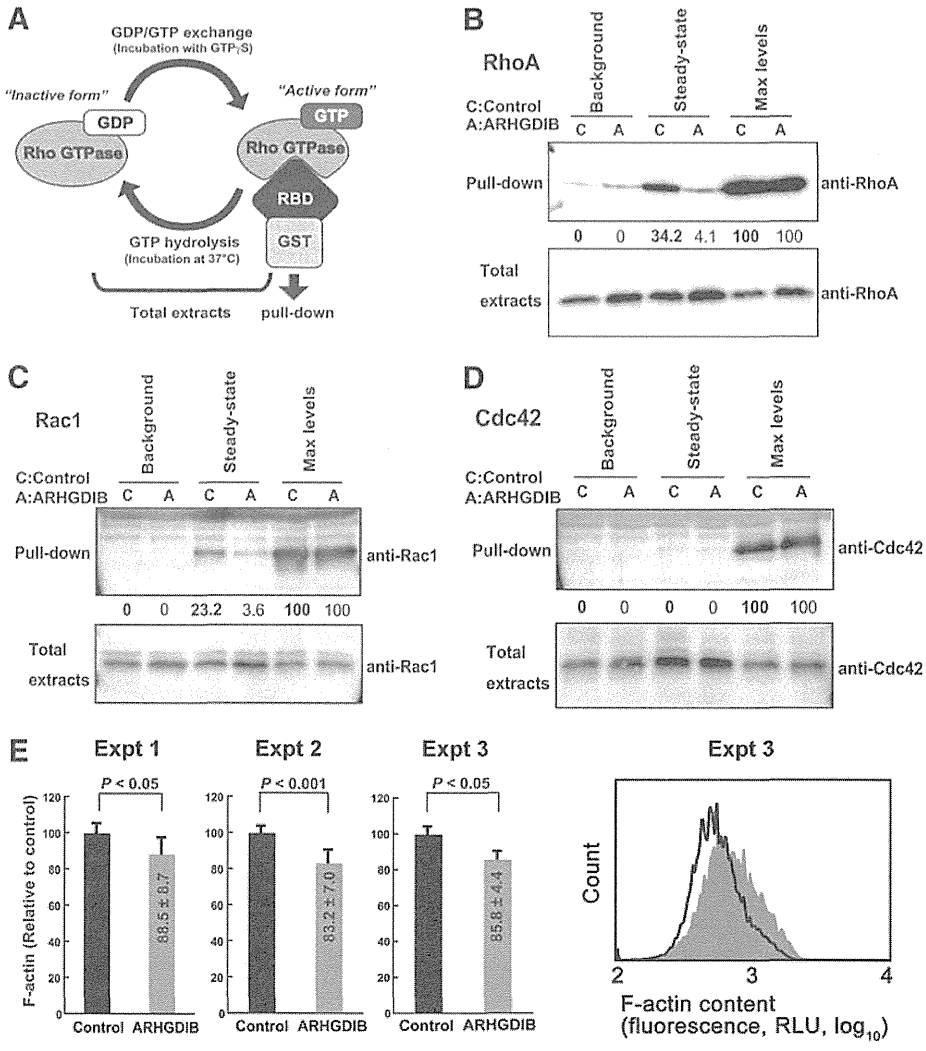

FIG. 2. Activation of RhoA and Rac1 under steady-state conditions in PM1 cells. **(A)** The experimental procedure for the active Rho GTPase capture assay. The active GTP-bound form is collected by glutathione-Sepharose beads coated with an RBD-GST fusion protein and compared with the total expression levels of each Rho GTPase by Western blot analysis. Incubation of the cell lysate with GTPγS shifts the equilibrium to the right, and incubation of the cell lysate at 37°C for 30 min shifts it to the left, representing the maximal activation levels (Max levels in **B–D**) or the background levels (background in **B–D**) of each Rho GTPase, respectively. **(B–D)** Activation of RhoA **(B)**, Rac1 **(C)**, and Cdc42 **(D)** in PM1 cells. The activation levels under steady-state conditions were estimated by densitometric analysis defined by setting the Max levels and background to 100% and 0%, respectively. **(E)** Measurement of F-actin content in PM1/ARHGDIB and control cells. Data from three independent experiments are shown in the bar graphs, and each of these experiments was performed in triplicate. The right panel shows the flow cytometric profile of Experiment 3, in which PM1/ARHGDIB is indicated by a black line, and the control is shown in gray. Statistical significance between the two groups was analyzed by two-tailed Student's *t*-test. AU, arbitrary unit.

reported previously.[31] This effect is modest in Cdc42 (1.1-fold, Fig. 2D) because the capture of Rho GTPase by ARHGDIB depends on the active GDP/GTP exchange cycle of Rho GTPase under steady-state conditions, which occurs inefficiently in Cdc42.

The common effector function of RhoA and Rac1 is the reorganization of the actin cytoskeleton.[11,12,32,33] If the ectopic expression of ARHGDIB inhibits RhoA and Rac1 effector function, the monomer-polymer actin equilibrium in ARHGDIB-transduced cells should be shifted toward a depolymerized state.[13,14,34] To test this, flow cytometry using fluorescently labeled phalloidin, which binds to F-actin, was used to measure the amount of polymerized actin. Under steady-state conditions, the fluorescence intensity of PM1/ARHGDIB cells was significantly lower than in control cells (Fig. 2E). The reduction levels of F-actin content in PM1/ARHGDIB cells were 14.2±1.6% ($N=3$, $p<0.05$ by Student's t-test, two-tailed; Fig. 2E) compared with the control. A similar trend was observed in SUP-T1 cells. These data are in agreement with the results obtained by the active Rho GTPase capture assay and the previous findings that the overexpression of RhoGDI in various cell lines induces the disruption of actin cytoskeleton-dependent processes.[35–37] These data indicate that the ectopic expression of ARHGDIB in T cells suppresses the activation status of both RhoA and Rac1 under steady-state tissue culture conditions.

Analysis of the viral life cycle in ARHGDIB-expressing T cells

Next, the mechanism by which ARHGDIB blocks HIV-1 replication was investigated. To do this, the viral entry and production phases were examined separately.

To examine the viral entry phase, PM1/ARHGDIB cells were infected with X4-tropic HIV-1_{NL4-3} Env- or VSV-G-pseudotyped HIV-1 that produces luciferase upon the establishment of infection. In these viruses, luciferase is under the regulation of a long terminal repeat (LTR) or cytomegalovirus (CMV) promoter. When the relative luciferase activity in the control cells was set at 100%, the infection efficiency of HIV-1 Env-pseudotyped HIV-1 expressing luciferase driven by the HIV-1 LTR promoter was 33.0±2.6% ($N=3$, $p<0.001$ by Student's t-test, two-tailed; Fig. 3A). Similar results were observed in MT-4 cells (data not shown). In contrast, the infection efficiency of VSV-G-pseudotyped HIV-1 expressing luciferase with either the HIV-1 LTR or CMV promoter was 243.2±31.9% ($N=3$, $p<0.01$; Fig. 3A) or 480.3±158.1% ($N=3$, $p<0.05$; Fig. 3A), respectively. Similarly, infection with VSV-G-pseudotyped MLV driving the expression of luciferase with the MLV LTR promoter was 10.0±6.4-fold more efficient in PM1/ARHGDIB than in control cells ($N=4$, $p<0.05$; Fig. 3A). To examine the effect of ARHGDIB on gene expression, reporter plasmids driving the expression of luciferase with either the CMV or HIV-1 LTR promoter were transfected into PM1 cells. The LTR- and CMV-driven luciferase activities in PM1/ARHGDIB cells were modestly increased compared with the control cells, but not decreased (2.1±0.6-fold, and 2.4±1.6-fold for LTR- and CMV-driven constructs, six and four independent experiments, respectively; Fig. 3B). Taken together, these data suggest that the inhibition of viral entry is specific to HIV-1 Env, and the early phase of the viral life cycle is strongly affected.

When measured by flow cytometry, PM1/ARHGDIB cells were found to express cell surface CD4 at levels 1.4-fold higher than control cells (average of four independent experiments), while the cell surface levels of CXCR4 were 0.8-fold higher (average of five independent experiments). Considering that ARHGDIB did not affect the levels of cell surface CD4 or CXCR4 in MT-4 cells (Fig. 1B) and M8166 cells (data not shown), and that the reduction in CXCR4 expression in PM1 cells is relatively modest, these data suggest that changes in the expression of viral receptors do not fully account per se for the decreased susceptibility of PM1/ARHGDIB cells to HIV-1_{NL4-3} Env-pseudotyped HIV-1.

To examine the production phase, proviral DNA was transfected into PM1/ARHGDIB and the control cells, and the viral protein expression in cells and the level of viral production in the culture supernatant were measured. The transfected cells were cultured in the presence of the antiretroviral drug efavirenz, which inhibits the replication cycle of HIV-1, allowing the assessment of viral production in the transfected cells. The levels of viral Gag in PM1/ARHGDIB cells, which are cleaved by protease to yield multiple bands in Western blot analysis with an anti-$p24^{CA}$ antibody, were comparable to the control cells (Fig. 3C). To assess these data quantitatively, densitometric analysis was conducted to quantify the signals representing $Pr55^{Gag}$, MA-CA, and $p24^{CA}$. Then, the percentage of $p24^{CA}$ and MA-CA relative to the total signal was calculated; this represented the efficiency of Gag processing. The Gag processing efficiency was 75.5% in PM1/ARHGDIB cells, similar to the control cells (69.9%). In addition, the ratio of the total signal in the viral lysate to that in the cell lysate was calculated. This reflects the efficiency of viral production. The virus/cell intensity ratios were 0.43 and 0.56 for the controls and cells ectopically expressing ARHGDIB, respectively. Similar data were obtained in an independent experiment in PM1 cells. These data suggest that the negative effect of ARHGDIB on the viral production phase was undetectable in T cells.

A single-round HIV-1 infection experiment was performed in the presence of a specific ROCK inhibitor, Y27632, to test whether the effector functions of RhoA are critical in regulating HIV-1 infection. The inhibition of ROCK, a RhoA signal mediator, reduced HIV-1 infection by 48.6±6.3% compared with the control levels ($N=4$, $p<0.05$ by Student's t-test, two-tailed; Fig. 3D). These observations suggested that the RhoA signal triggered by HIV-1 Env-receptor interaction is involved in the regulation of HIV-1 infection. This inhibition of ROCK accounted for approximately 77% of the inhibition of HIV-1 infection in PM1 cells ectopically expressing ARHGDIB (33.0% vs. 48.6%; Fig. 3A and D). These data also suggested that Rac1 plays a supplementary role in the restriction of HIV-1 infection. Taken together, this suggests that ARHGDIB limits HIV-1 replication primarily by affecting Env-mediated processes, most likely via receptor clustering and virus-cell membrane fusion.

Discussion

A handful of lymphoid-specific cellular regulators of HIV-1 replication are known, including CD4 and CCR5. However, few hematopoietic lineage-specific inhibitors of HIV-1 replication have been identified. Recently a dendritic- and myeloid-cell-specific restriction factor SAMHD1 has been

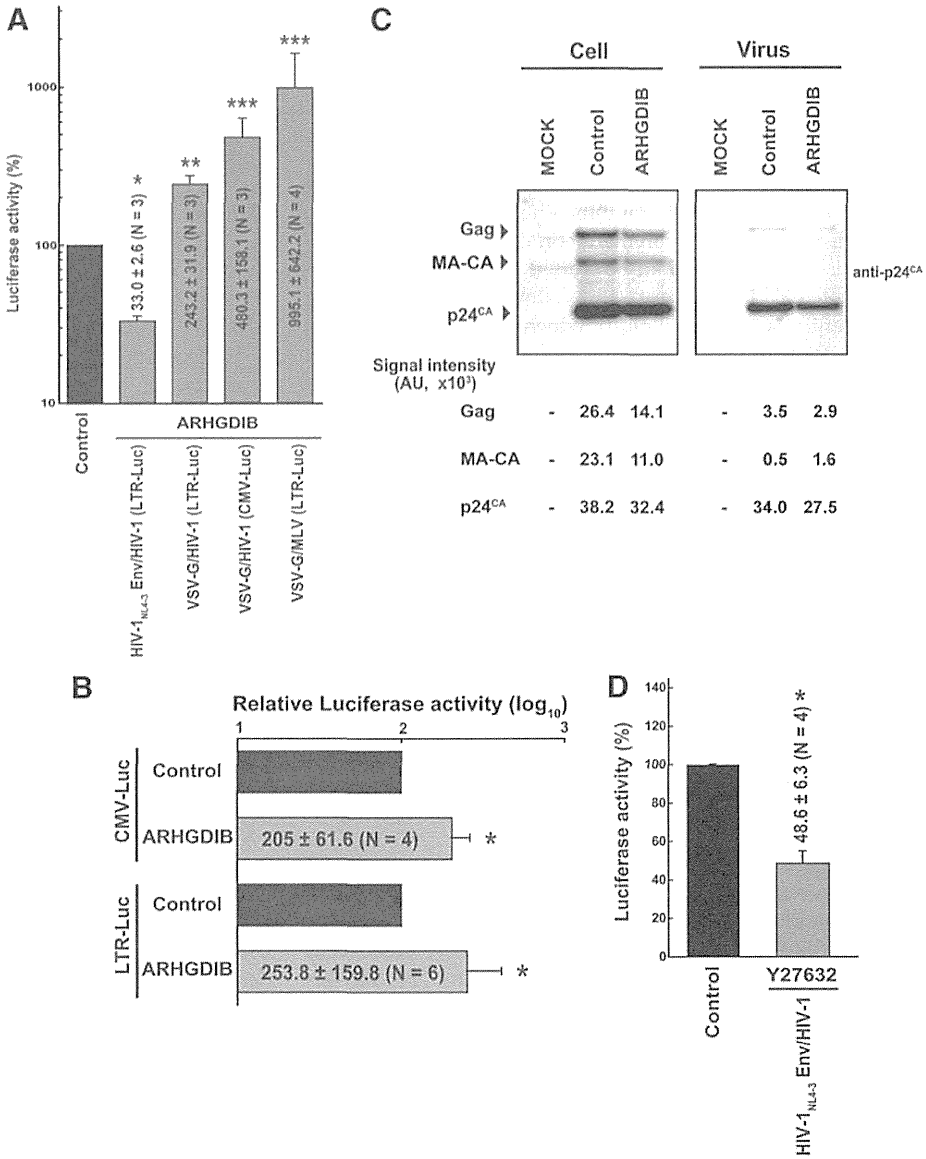

FIG. 3. The effect of ARHGDIB expression on the HIV-1 life cycle. **(A)** Single-round infection assay using replication-incompetent HIV-1 and MLV expressing luciferase upon integration, pseudotyped either with HIV-1 Env or with VSV-G. The promoters driving the expression of luciferase are noted in parentheses. Luciferase signals detected in PM1/ARHGDIB cells (gray) relative to control cells (black) are shown. The data represent the average and standard deviation from three or four independent experiments. Statistical significance between each group and the control was analyzed by two-tailed Student's *t*-test (single asterisk, $p < 0.001$; double asterisk, $p < 0.01$; and triple asterisk, $p < 0.05$). **(B)** Transient transfection assay to assess the effect of ARHGDIB on reporter gene expression. CMV- or HIV-1 LTR-driven luciferase expression vectors were introduced into PM1/control or PM1/ARHGDIB cells. Luciferase signals detected in PM1/ARHGDIB cells (gray) relative to control cells (black) are shown. The average and standard deviation from four and six independent experiments for CMV and LTR constructs, respectively, are shown. Statistical significance between PM1/ARHGDIB and the control was analyzed by two-tailed Student's *t*-test (asterisk, $p < 0.05$). **(C)** Viral production was assessed by transfecting proviral DNA into PM1/ARHGDIB and control cells. Viral protein levels in the cell lysate (Cell) and the pellet from the culture supernatant (Virus) were measured by Western blot analysis using anti-p24^{CA} monoclonal antibody. The expression levels of Gag, MA-CA and p24^{CA} were assessed by densitometric analysis and are shown in the lower panel. **(D)** Single-round infection assay in the presence of a ROCK inhibitor, Y27632. Luciferase signals detected in PM1/ARHGDIB cells (gray) relative to control cells (black) are shown. The data represent the average and standard deviation from four independent experiments. Statistical significance between each group and the control was analyzed by two-tailed Student's *t*-test (asterisk, $p < 0.05$).

reported.[38] APOBEC3 family members, which exhibit antiretroviral activity, may be hematopoietic cell specific, although their expression levels in non-T cells have not been directly examined.[39,40] In this study, we showed that modest up-regulation of the hematopoietic cell-specific RhoGDI, ARHGDIB, negatively regulated HIV-1 replication in various T cell lines, while it appeared to have no impact on cell proliferation. ARHGDIB is a constitutively expressed, lymphoid-specific protein. Therefore, ARHGDIB could provide intrinsic immunity against HIV-1 infection. In contrast, APOBEC3 family members are primarily interferon inducible.

RhoGDIs have not been isolated as negative regulators of HIV-1 replication in previous genetic screening studies. This is partly because nonlymphoid cells were used to screen genetic materials and the siRNA/shRNA-based gene knockdown is not able to identify negative regulators of HIV-1 replication at high sensitivity. Moreover, previous screens could not identify all potential factors, especially those present in the hematopoietic cell lineage, since nonlymphoid cells were often used. Our T cell-based screen using replication-competent HIV-1 allowed us to identify ARHGDIB as an HIV-1 inhibitor.

Rho GTPases play multiple roles in cell biology, including actin reorganization, endocytosis, and tubulin regulation, and ARHGDIB is a negative regulator of Rho GTPases.[11–14,32,41,42] It has been reported previously that inhibition of RhoA affects

viral receptor clustering, which lowers the efficiency of virus-cell membrane fusion and thus affects viral replication.[4,43–45] In contrast, the Rac1-PAK pathway has been shown to support virus-cell membrane fusion.[46,47] Both processes require active actin reorganization.[4,42,44–47] Interestingly, HIV-1 Env-guided entry is supported by a Filamin A-RhoA-ROCK axis and Arp2/3 complex, both of which are commonly involved in actin cytoskeletal reorganization.[21,44] Our data link the reported functions of RhoA, Rac1, and RhoGDIs with the biological phenotype of ARHGDIB; inhibition of HIV-1 replication in T cells. This HIV-1 inhibitory function of ARHGDIB is exerted via simultaneous functional restriction of two Rho GTPases, RhoA and Rac1. It is likely that receptor clustering and virus-cell membrane fusion are affected in T cells ectopically overexpressing ARHGDIB. As receptor clustering is the initial event of the HIV-1 life cycle, HIV-1 replication is attenuated in such cells regardless of the route of HIV-1 entry. Also, in T cells ectopically overexpressing ARHGDIB, RhoA and Rac1 are substantially inactivated. However, they are not inactivated completely. Thus, these cells are still able to support HIV-1 replication at certain levels, contributing to the delayed HIV-1 replication phenotype in cells ectopically overexpressing ARHGDIB.

Some reports suggest that RhoA inhibits LTR-mediated transcription.[43,48,49] If this is the case, increased ARHGDIB expression should enhance LTR-mediated transcription. In PM1/ARHGDIB cells, HIV-1 LTR-driven luciferase activity was slightly enhanced (Fig. 3B), which is consistent with previously reported findings. On the other hand, HIV-1 replication was repressed in T cells, suggesting that this transcriptional effect on viral replication is modest, if it occurs at all. It is also possible that the enhancement of the luciferase signal may be due to increased endocytic activity in PM1/ARHGDIB cells, since the DEAE-Dextran protocol was employed for transfection, and similar levels of enhancement of CMV-driven transcription were observed in PM1/ARHGDIB cells as well.

Infection with VSV-G-pseudotyped HIV-1 and MLV, which enter cells via endocytosis accompanied by the rearrangement of actin filaments, is augmented in PM1/ARHGDIB cells (Fig. 3A). These findings are consistent with a previous report demonstrating that ARHGDIB stimulates endocytosis in cells with a lymphoid background.[50] The efficiency of VSV-G-pseudotyped MLV infection into PM1/ARHGDIB cells was higher than VSV-G-pseudotyped HIV-1. During the entry phase, HIV-1 utilizes microtubules to traffic toward the nucleus, whereas MLV does not seem to actively do so.[51,52] As ARHGDIB potentially inhibits Rho GTPases, thereby disturbing microtubular organization, it is possible that HIV-1 infection is blocked by ARHGDIB at the microtubule-dependent transport phase in addition to the receptor clustering phase. Alternatively, the relatively high infectious titers produced by the MLV vector may be responsible for the observed phenotype.

Our findings do not negate the possibility that ARHGDIB limits HIV-1 replication by restricting the functions of other effector molecules. For instance, ARHGDIB has also been shown to bind the RhoGEF protein Vav1 and the cytoskeletal protein ezrin, both of which have been implicated in the positive regulation of HIV-1 replication.[53–57] Thus, these factors may also contribute to the ARHGDIB-mediated inhibition of HIV-1 replication.

The treatment efficacy of HIV-1/AIDS by antiretroviral drugs has greatly improved. However, the adverse effects of antiretroviral drugs lower the quality of life of HIV-1-infected individuals, and the emergence of drug-resistant strains is anticipated for all of the currently available antiretroviral drugs. Insights into HIV-1-host interaction, such as that provided in this study, will aid in the design of novel antiretroviral drugs. Our findings may contribute not only to antiretroviral drug development but also to our understanding of viral pathogenesis. Considering the observation that a modest increase in ARHGDIB expression resulted in the inhibition of HIV-1 replication, it is possible that, at the later phase of HIV-1 infection, CD4-positive cells bearing higher levels of ARHGDIB may be selected. Thus, ARHGDIB levels may be useful as a progression marker of HIV-1 infection. HIV-1 disease progression may be delayed in individuals who have relatively high levels of ARHGDIB in CD4-positive T cells. These possibilities should be examined in future studies.

Acknowledgments

This work was supported in part by the Japan Human Science Foundation, the Japanese Ministry of Health, Labor and Welfare (Research on HIV/AIDS), and the Japanese Ministry of Education, Culture, Sports, Science and Technology (Priority Areas "Matrix of Infection Phenomena" 18073008).

Author Disclosure Statement

No competing financial interests exist.

References

1. Lu X, Wu X, Plemenitas A, *et al.*: CDC42 and Rac1 are implicated in the activation of the Nef-associated kinase and replication of HIV-1. Curr Biol 1996;6(12):1677–1684.
2. Cook JA, Albacker L, August A, and Henderson AJ: CD28-dependent HIV-1 transcription is associated with Vav, Rac, and NF-kappa B activation. J Biol Chem 2003;278(37):35812–35818.
3. Akasaki T, Koga H, and Sumimoto H: Phosphoinositide 3-kinase-dependent and -independent activation of the small GTPase Rac2 in human neutrophils. J Biol Chem 1999; 274(25):18055–18059.
4. del Real G, Jimenez-Baranda S, Mira E, *et al.*: Statins inhibit HIV-1 infection by down-regulating Rho activity. J Exp Med 2004;200(4):541–547.
5. Loomis RJ, Holmes DA, Elms A, Solski PA, Der CJ, and Su L: Citron kinase, a RhoA effector, enhances HIV-1 virion production by modulating exocytosis. Traffic 2006;7(12):1643–1653.
6. Pontow S, Harmon B, Campbell N, and Ratner L: Antiviral activity of a Rac GEF inhibitor characterized with a sensitive HIV/SIV fusion assay. Virology 2007;368(1):1–6.
7. Galandrini R, Henning SW, and Cantrell DA: Different functions of the GTPase Rho in prothymocytes and late pre-T cells. Immunity 1997;7(1):163–174.
8. Brown A, Wang X, Sawai E, and Cheng-Mayer C: Activation of the PAK-related kinase by human immunodeficiency virus type 1 Nef in primary human peripheral blood lymphocytes and macrophages leads to phosphorylation of a PIX-p95 complex. J Virol 1999;73(12):9899–9907.

9. Zhang B, Zhang Y, Dagher MC, and Shacter E: Rho GDP dissociation inhibitor protects cancer cells against drug-induced apoptosis. Cancer Res 2005;65(14):6054–6062.
10. Kolesnitchenko V, King L, Riva A, Tani Y, Korsmeyer SJ, and Cohen DI: A major human immunodeficiency virus type 1-initiated killing pathway distinct from apoptosis. J Virol 1997;71(12):9753–9763.
11. DerMardirossian C and Bokoch GM: GDIs: Central regulatory molecules in Rho GTPase activation. Trends Cell Biol 2005;15(7):356–363.
12. Dovas A and Couchman JR: RhoGDI: Multiple functions in the regulation of Rho family GTPase activities. Biochem J 2005;390(Pt 1):1–9.
13. Heasman SJ and Ridley AJ: Mammalian Rho GTPases: New insights into their functions from in vivo studies. Nat Rev Mol Cell Biol 2008;9(9):690–701.
14. Ladwein M and Rottner K: On the Rho'd: The regulation of membrane protrusions by Rho-GTPases. FEBS Lett 2008;582(14):2066–2074.
15. Brass AL, Dykxhoorn DM, Benita Y, *et al.:* Identification of host proteins required for HIV infection through a functional genomic screen. Science 2008;319(5865):921–926.
16. Zhou H, Xu M, Huang Q, *et al.:* Genome-scale RNAi screen for host factors required for HIV replication. Cell Host Microbe 2008;4(5):495–504.
17. Simmons A, Gangadharan B, Hodges A, *et al.:* Nef-mediated lipid raft exclusion of UbcH7 inhibits Cbl activity in T cells to positively regulate signaling. Immunity 2005;23(6):621–634.
18. Hodges A, Sharrocks K, Edelmann M, *et al.:* Activation of the lectin DC-SIGN induces an immature dendritic cell phenotype triggering Rho-GTPase activity required for HIV-1 replication. Nat Immunol 2007;8(6):569–577.
19. Urano E, Ichikawa R, Morikawa Y, Yoshida T, Koyanagi Y, and Komano J: T cell-based functional cDNA library screening identified SEC14-like 1a carboxy-terminal domain as a negative regulator of human immunodeficiency virus replication. Vaccine 2010;28(Suppl 2):B68–B74.
20. Urano E, Kariya Y, Futahashi Y, *et al.:* Identification of the P-TEFb complex-interacting domain of Brd4 as an inhibitor of HIV-1 replication by functional cDNA library screening in MT-4 cells. FEBS Lett 2008;582(29):4053–4058.
21. Komano J, Miyauchi K, Matsuda Z, and Yamamoto N: Inhibiting the Arp2/3 complex limits infection of both intracellular mature vaccinia virus and primate lentiviruses. Mol Biol Cell 2004;15(12):5197–5207.
22. Kimura K, Tsuji T, Takada Y, Miki T, and Narumiya S: Accumulation of GTP-bound RhoA during cytokinesis and a critical role of ECT2 in this accumulation. J Biol Chem 2000;275(23):17233–17236.
23. Takahashi Y, Tanaka Y, Yamashita A, Koyanagi Y, Nakamura M, and Yamamoto N: OX40 stimulation by gp34/OX40 ligand enhances productive human immunodeficiency virus type 1 infection. J Virol 2001;75(15):6748–6757.
24. Vicente-Manzanares M, Viton M, and Sanchez-Madrid F: Measurement of the levels of polymerized actin (F-actin) in chemokine-stimulated lymphocytes and GFP-coupled cDNA transfected lymphoid cells by flow cytometry. Methods Mol Biol 2004;239:53–68.
25. Shimizu S, Urano E, Futahashi Y, *et al.:* Inhibiting lentiviral replication by HEXIM1, a cellular negative regulator of the CDK9/cyclin T complex. AIDS 2007;21(5):575–582.
26. Sato K, Aoki J, Misawa N, *et al.:* Modulation of human immunodeficiency virus type 1 infectivity through incorporation of tetraspanin proteins. J Virol 2008;82(2):1021–1033.
27. Togawa A, Miyoshi J, Ishizaki H, *et al.:* Progressive impairment of kidneys and reproductive organs in mice lacking Rho GDIalpha. Oncogene 1999;18(39):5373–5380.
28. Reif K and Cantrell DA: Networking Rho family GTPases in lymphocytes. Immunity 1998;8(4):395–401.
29. Tuosto L, Michel F, and Acuto O: p95vav associates with tyrosine-phosphorylated SLP-76 in antigen-stimulated T cells. J Exp Med 1996;184(3):1161–1166.
30. Stowers L, Yelon D, Berg LJ, and Chant J: Regulation of the polarization of T cells toward antigen-presenting cells by Ras-related GTPase CDC42. Proc Natl Acad Sci USA 1995;92(11):5027–5031.
31. Boulter E, Garcia-Mata R, Guilluy C, *et al.:* Regulation of Rho GTPase crosstalk, degradation and activity by RhoGDI1. Nat Cell Biol 2010;12(5):477–483.
32. Etienne-Manneville S and Hall A: Rho GTPases in cell biology. Nature 2002;420(6916):629–635.
33. Dransart E, Morin A, Cherfils J, and Olofsson B: RhoGDI-3, a promising system to investigate the regulatory function of rhoGDIs: uncoupling of inhibitory and shuttling functions of rhoGDIs. Biochem Soc Trans 2005;33(Pt 4):623–626.
34. Lee SH and Dominguez R: Regulation of actin cytoskeleton dynamics in cells. Mol Cells 2010;29(4):311–325.
35. Takaishi K, Kikuchi A, Kuroda S, Kotani K, Sasaki T, and Takai Y: Involvement of rho p21 and its inhibitory GDP/GTP exchange protein (rho GDI) in cell motility. Mol Cell Biol 1993;13(1):72–79.
36. Miura Y, Kikuchi A, Musha T, *et al.:* Regulation of morphology by rho p21 and its inhibitory GDP/GTP exchange protein (rho GDI) in Swiss 3T3 cells. J Biol Chem 1993;268(1):510–515.
37. Komuro R, Sasaki T, Takaishi K, Orita S, and Takai Y: Involvement of Rho and Rac small G proteins and Rho GDI in Ca2+-dependent exocytosis from PC12 cells. Genes Cells 1996;1(10):943–951.
38. Laguette N, Sobhian B, Casartelli N, *et al.:* SAMHD1 is the dendritic- and myeloid-cell-specific HIV-1 restriction factor counteracted by Vpx. Retrovirology 2011;474(7353):654–657.
39. Koning FA, Newman EN, Kim EY, Kunstman KJ, Wolinsky SM, and Malim MH: Defining APOBEC3 expression patterns in human tissues and hematopoietic cell subsets. J Virol 2009;83(18):9474–9485.
40. Refsland EW, Stenglein MD, Shindo K, Albin JS, Brown WL, and Harris RS: Quantitative profiling of the full APOBEC3 mRNA repertoire in lymphocytes and tissues: Implications for HIV-1 restriction. Nucleic Acids Res 2010;38(13):4274–4284.
41. Ridley AJ: Rho GTPases and cell migration. J Cell Sci 2001;114(Pt 15):2713–2722.
42. Fukata M, Nakagawa M, and Kaibuchi K: Roles of Rho-family GTPases in cell polarisation and directional migration. Curr Opin Cell Biol 2003;15(5):590–597.
43. Iyengar S, Hildreth JE, and Schwartz DH: Actin-dependent receptor colocalization required for human immunodeficiency virus entry into host cells. J Virol 1998;72(6):5251–5255.
44. Jimenez-Baranda S, Gomez-Mouton C, Rojas A, *et al.:* Filamin-A regulates actin-dependent clustering of HIV receptors. Nat Cell Biol 2007;9(7):838–846.
45. Malinowsky K, Luksza J, and Dittmar MT: Susceptibility to virus-cell fusion at the plasma membrane is reduced through expression of HIV gp41 cytoplasmic domains. Virology 2008;376(1):69–78.
46. Pontow SE, Heyden NV, Wei S, and Ratner L: Actin cytoskeletal reorganizations and coreceptor-mediated activation

of rac during human immunodeficiency virus-induced cell fusion. J Virol 2004;78(13):7138–7147.
47. Harmon B and Ratner L: Induction of the Galpha(q) signaling cascade by the human immunodeficiency virus envelope is required for virus entry. J Virol 2008;82(18):9191–9205.
48. Wang L, Zhang H, Solski PA, Hart MJ, Der CJ, and Su L: Modulation of HIV-1 replication by a novel RhoA effector activity. J Immunol 2000;164(10):5369–5374.
49. Helms WS, Jeffrey JL, Holmes DA, Townsend MB, Clipstone NA, and Su L: Modulation of NFAT-dependent gene expression by the RhoA signaling pathway in T cells. J Leukoc Biol 2007;82(2):361–369.
50. Lamaze C, Chuang TH, Terlecky LJ, Bokoch GM, and Schmid SL: Regulation of receptor-mediated endocytosis by Rho and Rac. Nature 1996;382(6587):177–179.
51. Sodeik B: Unchain my heart, baby let me go—the entry and intracellular transport of HIV. J Cell Biol 2002;159(3):393–395.
52. Naghavi MH and Goff SP: Retroviral proteins that interact with the host cell cytoskeleton. Curr Opin Immunol 2007;19(4):402–407.
53. Haedicke J, de Los Santos K, Goff SP, and Naghavi MH: The Ezrin-radixin-moesin family member ezrin regulates stable microtubule formation and retroviral infection. J Virol 2008;82(9):4665–4670.
54. Hecker C, Weise C, Schneider-Schaulies J, Holmes HC, and ter Meulen V: Specific binding of HIV-1 envelope protein gp120 to the structural membrane proteins ezrin and moesin. Virus Res 1997;49(2):215–223.
55. Kubo Y, Yoshii H, Kamiyama H, *et al.:* Ezrin, Radixin, and Moesin (ERM) proteins function as pleiotropic regulators of human immunodeficiency virus type 1 infection. Virology 2008;375(1):130–140.
56. Barrero-Villar M, Cabrero JR, Gordon-Alonso M, *et al.:* Moesin is required for HIV-1-induced CD4-CXCR4 interaction, F-actin redistribution, membrane fusion and viral infection in lymphocytes. J Cell Sci 2009;122(Pt 1):103–113.
57. Fackler OT, Luo W, Geyer M, Alberts AS, and Peterlin BM: Activation of Vav by Nef induces cytoskeletal rearrangements and downstream effector functions. Mol Cell 1999;3(6):729–739.

Address correspondence to:
Jun Komano
AIDS Research Center
National Institute of Infectious Diseases
1-23-1 Toyama, Shnjuku
Tokyo 162-8640
Japan

E-mail: ajkomano@nih.go.jp

JVI
Journals.ASM.org

Vpu Augments the Initial Burst Phase of HIV-1 Propagation and Downregulates BST2 and CD4 in Humanized Mice

Kei Sato,[a] Naoko Misawa,[b] Mitsuko Fukuhara,[b,d] Shingo Iwami,[b,c,e,f]* Dong Sung An,[g,h,i] Mamoru Ito,[j] and Yoshio Koyanagi[a,b]

Center for Emerging Virus Research,[a] Laboratory of Viral Pathogenesis,[b] and Laboratory of Primate Model,[c] Institute for Virus Research, Kyoto University, Sakyo-ku, Kyoto, Japan; Faculty of Science, Kyoto University, Kitashirakawaoiwake-cho, Sakyo-ku, Kyoto, Japan[d]; Precursory Research for Embryonic Science and Technology, Japan Science and Technology Agency, Kawaguchi, Saitama, Japan[e]; Graduate School of Mathematical Sciences, The University of Tokyo, Meguro-ku, Tokyo, Japan[f]; Division of Hematology-Oncology,[g] School of Nursing,[h] and AIDS Institute,[i] University of California, Los Angeles, Los Angeles, California, USA; and Central Institute for Experimental Animals, Kawasaki-ku, Kawasaki, Kanagawa, Japan[j]

While human cells express potent antiviral proteins as part of the host defense repertoire, viruses have evolved their own arsenal of proteins to antagonize them. BST2 was identified as an inhibitory cellular protein of HIV-1 replication, which tethers virions to the cell surface to prevent their release. On the other hand, the HIV-1 accessory protein, Vpu, has the ability to downregulate and counteract BST2. Vpu also possesses the ability to downmodulate cellular CD4 and SLAMF6 molecules expressed on infected cells. However, the role of Vpu in HIV-1 infection *in vivo* remains unclear. Here, using a human hematopoietic stem cell-transplanted humanized mouse model, we demonstrate that Vpu contributes to the efficient spread of HIV-1 *in vivo* during the acute phase of infection. Although Vpu did not affect viral cytopathicity, target cell preference, and the level of viral protein expression, the amount of cell-free virions in *vpu*-deficient HIV-1-infected mice was profoundly lower than that in wild-type HIV-1-infected mice. We provide a novel insight suggesting that Vpu concomitantly downregulates BST2 and CD4, but not SLAMF6, from the surface of infected cells. Furthermore, we show evidence suggesting that BST2 and CD4 impair the production of cell-free infectious virions but do not associate with the efficiency of cell-to-cell HIV-1 transmission. Taken together, our findings suggest that Vpu downmodulates BST2 and CD4 in infected cells and augments the initial burst of HIV-1 replication *in vivo*. This is the first report demonstrating the role of Vpu in HIV-1 infection in an *in vivo* model.

Human immunodeficiency virus type 1 (HIV-1), the causative agent of AIDS, encodes four accessory proteins in its viral genome: negative factor (Nef), virus infectivity factor (Vif), vial protein R (Vpr), and viral protein U (Vpu) (10). Vpu is a 16-kDa integral membrane protein and is expressed from a bicistronic mRNA together with envelope protein (Env) during the late stage of the viral life cycle (10, 65). Vpu was originally acquired by the ancestor of certain simian immunodeficiency viruses (SIVs; SIVmon, SIVmus, and SIVgsn) and was later transferred to SIVcpz and HIV-1 by recombination and cross-species transmission events. On the other hand, Vpu is noticeably absent in human immunodeficiency virus type 2 (HIV-2) and the other SIVs including SIVsmm/mac (7, 26).

Vpu has been found to act on several cellular proteins by affecting their surface expression using two common mechanisms: (i) targeting them for ubiquitin-mediated degradation and/or (ii) trafficking them from the plasma membrane to intracellular compartments. It is widely known that Vpu can recruit β-transducin repeat-containing protein 1 (BTRC; also called β-TrCP1), an E3 ubiquitin ligase, and degrades CD4 molecules by the ubiquitin/proteasome pathway (31, 35, 60, 72). In addition, a recent report demonstrated that signaling lymphocyte activation molecule family member 6 (SLAMF6; also called NTB-A), a transmembrane protein that induces natural killer cell-mediated killing, can be downregulated from the plasma membrane by Vpu (64).

A third molecule influenced by Vpu was discovered after observations that different cell types displayed various degrees of viral replication kinetics after HIV-1 infection with or without Vpu. Virus yields in the supernatant of *vpu*-deficient HIV-1-infected/transfected cells were reported to be lower than those of *vpu*-proficient (i.e., wild-type [WT]) HIV-1-infected/transfected cells in certain $CD4^+$ T cell lines (41, 61), primary $CD4^+$ T cells (41, 61–63), monocyte-derived macrophages (59, 62, 63, 66), *in vitro* tonsil histocultures (59), and HeLa cells (12). However, Vpu was dispensable for HIV-1 virion production in cell lines such as 293T cells and HT1080 cells. Varthakavi et al. later demonstrated that HeLa cells express an inhibitory factor for HIV-1 particle release, which can be counteracted by Vpu (68). In 2008, Neil et al. (42) and Van Damme et al. (67) identified this factor as tetherin and bone marrow stromal cell antigen 2 (BST2; also known as CD317 or HM1.24), respectively. BST2 is a glycosylphosphatidylinositol-anchored transmembrane protein and is endogenously expressed in human $CD4^+$ T cells and macrophages (9). Van Damme et al. (67) and other groups, including ours (56), have reported that BST2 expressed on the surface of HIV-1-infected cells is severely downregulated by Vpu. Moreover, some reports have revealed that Vpu-mediated BST2 downregulation is dependent on BTRC, similar to the manner by which CD4 is downregulated (7, 8, 11, 37).

The restriction conferred by BST2 is not limited to retroviruses (9, 23, 26) but also various enveloped viruses belonging to *Filoviridae* (Ebola virus and Marburg virus) (23, 24, 49), *Arenaviridae*

Received 8 December 2011 Accepted 11 February 2012
Published ahead of print 22 February 2012
Address correspondence to Yoshio Koyanagi, ykoyanag@virus.kyoto-u.ac.jp.
* Present address: Department of Biology, Faculty of Sciences, Kyushu University, Higashi-ku, Fukuoka, Japan.

doi:10.1128/JVI.07062-11

(Lassafever virus) (49), *Herpesviridae* (Kaposi's sarcoma-associated herpesvirus) (34), *Rhabdoviridae* (vesicular stomatitis virus) (71), *Orthomyxoviridae* (influenza A virus) (69), and *Paramyxoviridae* (Nipah virus) (47). However, some of these viruses possess their own antagonizing BST2 counterparts instead of Vpu. For instance, HIV-2 counteracts BST2 with its envelope glycoprotein (Env) (8, 13, 15, 30), while SIVsmm/mac impairs the tethering function of simian BST2 with its accessory protein, Nef (15, 58, 73). In addition, it was reported that Ebola virus glycoprotein (24) and the K5 protein of Kaposi's sarcoma-associated herpesvirus (34, 46) can counteract BST2. Given that various diverse viruses have evolved methods to overcome the restriction by BST2, it would appear that its tethering ability is critical for the host defense.

Lines of investigations in cell culture systems have revealed the molecular mechanisms of virion tethering by BST2 and the ability of Vpu to antagonize BST2, which have shed light on host-virus interactions. Moreover, accumulating evidence suggests that BST2 is a potent suppressor of HIV-1 infection. However, the role of Vpu in HIV-1 expansion *in vivo*, particularly its antagonism of BST2 *in vivo*, remains unresolved.

In order to elucidate the dynamics of human-specific pathogens such as HIV-1 *in vivo*, we have constructed a humanized mouse model by xenotransplanting human $CD34^+$ hematopoietic stem cells into an immunodeficient NOD/SCID *Il2rg*$^{-/-}$ (NOG) mouse (44, 52, 55). In this system, human leukocytes including human $CD4^+$ T cells are differentiated *de novo* and are stably and longitudinally maintained. By using these humanized mice, we have established novel animal models for HIV-1 and Epstein-Barr virus infections and related diseases (44, 52, 54, 55). Particularly noteworthy is that our humanized mice, named NOG-hCD34 mice, are able to recapitulate the characteristics of HIV-1 pathogenesis, such as the depletion of $CD4^+$ T cells in peripheral blood (PB) and the preferential infection of effector memory $CD4^+$ T cells (44, 53).

In this study, by utilizing our humanized mouse model, we show that Vpu positively associates with efficient HIV-1 replication *in vivo* during the initial phase of infection. In addition, we investigated the dynamics of three Vpu-associated cellular proteins, BST2, CD4, and SLAMF6, *in vivo* and found that BST2 and CD4 but not SLAMF6 were severely downregulated on the surface of infected cells in a Vpu-dependent manner. Moreover, immunostaining analyses revealed frequent cell-to-cell interaction of HIV-1-infected cells in the spleen of infected mice, suggesting the occurrence of an efficient cell-to-cell virus transmission *in vivo*. Furthermore, *in vitro* transfection experiments demonstrated that BST2 and CD4 distinctively and synergistically suppressed the production of infectious virions while modestly affecting the efficiency of cell-to-cell infection. This is the first report focusing on the fundamental role of Vpu in HIV-1 infection *in vivo*. Our findings suggest that Vpu enhances the kinetics of cell-free virus propagation, especially during the initial phase of infection, and downregulates BST2 and CD4 in infected cells, which lead to a rapid systemic HIV-1 dissemination *in vivo*.

MATERIALS AND METHODS

Ethics statement. All protocols involving human subjects were reviewed and approved by the Kyoto University institutional review board. Informed written consent from the human subjects was obtained in this study.

Humanized mice. NOD.Cg-*Prkdc*^{scid} *Il2rg*^{tm1Sug}/Jic (NOD/SCID *Il2rg*$^{-/-}$) mice (14) were obtained from the Central Institute for Experimental Animals (Kanagawa, Japan). The mice were maintained under specific-pathogen-free conditions and were handled in accordance with the Regulation on Animal Experimentation at Kyoto University. Human $CD34^+$ hematopoietic stem cells were isolated from human fetal liver as described previously (1). The humanized mouse (NOG-hCD34 mouse) was constructed as previously described (44, 52, 54, 55). Briefly, 70 newborn (aged 0 to 2 days) NOG mice from 15 litters were irradiated with X-ray (10 cGy per mouse) by an RX-650 X-ray cabinet system (Faxitron X-ray Corporation) and were then intrahepatically injected with the obtained human $CD34^+$ cells (12×10^4 to 35×10^4 cells). A list of the humanized mice used in this study is summarized in Table 1.

Cell culture. 293T cells, HeLa cells, HEK293 cells, and TZM-bl cells (obtained through the NIH AIDS Research and Reference Reagent Program) (70) were maintained in Dulbecco's modified Eagle medium (DMEM) containing 10% fetal calf serum, 100 U/ml penicillin, and 100 μg/ml streptomycin as previously described (27, 51, 52, 56). Primary human $CD4^+$ T cells were isolated from the peripheral blood of a healthy donor by using a human $CD4^+$ T cell isolation kit (Miltenyi) according to the manufacturer's protocol. The isolated cells were stimulated with Dynabeads Human T-Activator CD3/CD28 for cell expansion and activation (Invitrogen) for 3 days. The activated human $CD4^+$ T cells were maintained in RPMI 1640 medium containing 10% fetal calf serum, 100 U/ml interleukin-2, 100 U/ml penicillin, and 100 μg/ml streptomycin.

Transfection, Western blotting, and TZM-bl assay. For *in vitro* transfection experiments shown in Fig. 1, 1 μg of pAD8$^+$ (a molecular clone of HIV-1 strain AD8 [HIV-1_{AD8}]) (66), pAD8-U_{DEL2}, which is a derivative of AD8 carrying an 81-bp deletion and an 8-bp irrelevant insertion in the *vpu* region (62, 63), or pUC19 (for mock control [TaKaRa]; shown as "vector" on the figures) was transfected into 293T and HeLa cells by using Lipofectamine 2000 (Life Technologies) according to the manufacturer's protocol. At 48 h posttransfection, the culture supernatant was harvested, centrifuged, and then filtered through a 0.45-μm-pore-size filter (Millipore) to produce virus solutions. To detect viral and cellular proteins, Western blotting was performed as previously described (27, 51, 52, 56). For Western blotting, the following antibodies were used: goat anti-p24 polyclonal antibody (Virostat), rabbit anti-Vpu polyclonal antibody (U2-3; kindly provided by Klaus Strebel) (33), and mouse anti-α-tubulin (TUBA) monoclonal antibody (DM1A; Sigma). To quantify the infectivities of the obtained viruses, a TZM-bl assay was performed as previously described (56). For *in vitro* transfection experiments shown in Fig. 9, a BST2 expression plasmid (pBST2) and a CD4 expression plasmid (pCD4), which are based on pCMV-SPORT6 (Invitrogen), were prepared. To construct pBST2, a *BST2* cDNA was obtained from pKGC-BST2 (27), and the obtained fragment was inserted into pCMV-SPORT6. To construct a CD4 expression plasmid (pCD4), pBCMGSNeo-human CD4 (kindly donated by Masayuki Miyasaka) was digested with XhoI, blunted, and then further digested with NotI. The resulting fragment was inserted into the EcoRV-XhoI site of pCMV-SPORT6. Sequences of these plasmid constructs were confirmed with an ABI Prism 3130xl genetic analyzer (Applied Biosystems). A total of 800 ng of pAD8$^+$, pAD8-U_{DEL2}, or pUC19 (for mock control; termed vector on the figures) was cotransfected with either 10 nanograms of pBST2 or pCD4 or both into HEK293 cells by using Lipofectamine 2000. A total of 100 ng of a green fluorescent protein (GFP)-expressing plasmid, peGFP-C1 (Clontech), was also cotransfected to monitor transfection efficiency, and DNA content in each well was adjusted to 1 μg by using pCMV-SPORT6. At 48 h posttransfection, the culture supernatant was harvested, centrifuged, and then filtered through a 0.45-μm-pore-size filter to produce virus solutions. The transfected cells were washed and suspended with DMEM, and 1/10 of the cell suspension was cocultured with TZM-bl cells. The TZM-bl assay was performed as described above.

Virus preparation and infection. To prepare the virus solutions of WT HIV-1_{AD8} and *vpu*-deficient HIV-1_{AD8} (HIV-1Δ*vpu*) for the experi-

TABLE 1 Humanized mice used in this study[a]

Mouse no.[b]	Recipient mouse		Transplanted hHSCs[c]		Inoculated virus	Dose ($\times 10^3$ $TCID_{50}$)	Inoculation age (no. of wks)
	Lot no.[c]	Sex[a]	Donor lot[d]	No. of cells			
1	104	M	A	170,000	HIV-1Δ*vpu*	300	15
2	105	F	B	140,000			14
3	105	M	B	140,000	HIV-1Δ*vpu*	300	14
4	105	M	B	140,000			14
5	105	M	B	140,000	HIV-1	300	14
6	105	M	B	140,000	HIV-1	300	14
7	106	F	C	120,000	HIV-1Δ*vpu*	300	14
8	106	F	C	120,000			14
9	106	M	C	120,000	HIV-1	300	14
10	106	M	C	120,000			14
11	106	M	C	120,000	HIV-1Δ*vpu*	300	14
12	108	F	D	240,000	HIV-1	300	13
13	108	F	D	240,000	HIV-1Δ*vpu*	300	13
14	108	F	D	240,000	HIV-1	300	13
15	108	M	D	240,000			13
16	108	M	D	240,000	HIV-1	300	13
17	108	M	D	240,000			13
18	108	M	D	240,000	HIV-1Δ*vpu*	300	13
19	109	F	E	350,000	HIV-1Δ*vpu*	300	12
20	109	F	E	350,000			12
21	109	M	E	350,000	HIV-1	300	12
22	110	M	F	300,000	HIV-1	300	15
23	110	M	F	300,000	HIV-1Δ*vpu*	300	15
24	110	M	F	300,000	HIV-1	300	15
25	113	F	E	300,000	HIV-1	300	15
26	113	F	E	300,000	HIV-1Δ*vpu*	300	15
27	113	M	E	200,000	HIV-1Δ*vpu*	300	14
28	113	M	E	200,000	HIV-1	300	14
29	113	M	E	200,000	HIV-1Δ*vpu*	300	14
30	114	F	D	180,000	HIV-1	300	17
31	114	M	D	180,000	HIV-1Δ*vpu*	300	17
32	116	F	F	250,000	HIV-1	300	15
33	116	F	F	250,000	HIV-1Δ*vpu*	300	15
34	116	M	F	250,000	HIV-1Δ*vpu*	300	15
35	116	M	F	250,000	HIV-1	300	15
36	117	F	C	170,000	HIV-1Δ*vpu*	300	15
37	117	F	C	170,000	HIV-1Δ*vpu*	300	15
38	117	F	C	170,000	HIV-1	300	15
39	117	F	C	170,000	HIV-1	300	15
40	117	M	C	170,000	HIV-1Δ*vpu*	300	15
41	117	M	C	170,000	HIV-1	300	15
42	117	M	C	170,000	HIV-1Δ*vpu*	300	15
43	117	M	C	170,000	HIV-1	300	15
44	130	F	D	130,000	HIV-1	3	14
45	130	F	D	130,000	HIV-1Δ*vpu*	3	14
46	126	F	G	130,000	HIV-1Δ*vpu*	3	14
47	126	F	G	130,000	HIV-1Δ*vpu*	3	14
48	126	F	G	130,000	HIV-1	3	14
49	126	F	G	130,000	HIV-1Δ*vpu*	3	14
50	126	M	G	130,000	HIV-1	30	14
51	126	M	G	130,000	HIV-1	30	14
52	126	M	G	130,000	HIV-1	300	14
53	126	M	G	130,000	HIV-1Δ*vpu*	30	14
54	127	F	G	130,000	HIV-1	300	14
55	127	F	G	130,000	HIV-1	3	14

(Continued on following page)

TABLE 1 (Continued)

Mouse no.[b]	Recipient mouse		Transplanted hHSCs[e]		Inoculated virus	Dose ($\times 10^3$ $TCID_{50}$)	Inoculation age (no. of wks)
	Lot no.[c]	Sex[a]	Donor lot[d]	No. of cells			
56	127	F	G	130,000	HIV-1	3	14
57	127	F	G	130,000	HIV-1Δ*vpu*	30	14
58	127	M	G	130,000	HIV-1	300	14
59	127	M	G	130,000	HIV-1Δ*vpu*	300	14
60	127	M	G	130,000	HIV-1Δ*vpu*	300	14
61	128	F	H	130,000	HIV-1	3	14
62	128	M	H	130,000	HIV-1	30	14
63	128	M	H	130,000	HIV-1Δ*vpu*	3	14
64	128	M	H	130,000	HIV-1Δ*vpu*	3	14
65	128	M	H	130,000	HIV-1	3	14
66	129	F	H	130,000	HIV-1	30	14
67	129	M	H	130,000	HIV-1	30	14
68	129	M	H	130,000	HIV-1Δ*vpu*	30	14
69	129	M	H	130,000	HIV-1Δ*vpu*	30	14
70	129	M	H	130,000	HIV-1Δ*vpu*	30	14

[a] M, male; F, female.
[b] Mouse numbers 11, 25, 26, 28, and 29 correspond with those shown in Fig. 3A.
[c] Fifteen lots of newborn NOG mice were used for the recipient.
[d] NOG-hCD34 mice were reconstituted with one of eight donors.
[e] hHSCs, human $CD34^+$ hematopoietic stem cells.

ments using humanized mouse, 30 μg of either $pAD8^+$ or $pAD8\text{-}U_{DEL2}$ was transfected into 293T cells by the calcium-phosphate method. At 48 h posttransfection, the culture supernatant was harvested, centrifuged, and then filtered through a 0.45-μm-pore-size filter to produce virus solution. To titrate virus infectivity, the virus solution obtained was serially diluted and then inoculated onto phytohemagglutinin-stimulated human peripheral blood mononuclear cells in a 96-well plate in triplicate. At 14 days postinfection, the endpoint was determined by using an HIV-1 p24 antigen enzyme-linked immunosorbent assay (ELISA) kit (ZetroMetrix), and virus infectivity was calculated as the 50% tissue culture infectious doses ($TCID_{50}$) according to the Reed-Muench method. The $TCID_{50}$ of WT and *vpu*-deficient HIV-1 used in this study were 7.74×10^6/ml and 7.72×10^6/ml, respectively. A virus solution of 3,000, 30,000, or 300,000 $TCID_{50}$ was intraperitoneally inoculated into NOG-hCD34 mice aged between 12 to 17 weeks old (Table 1). RPMI 1640 medium was used in mock infections.

PB collection and isolation of mononuclear cells from organs. PB and plasma were routinely collected as previously described (44). The spleen was crushed, rubbed, and suspended, and the bone marrow (BM) was obtained from the dissected thighbones by flushing the interior as previously described (44). The human mononuclear cells (MNCs) in the spleen and the BM were isolated as previously described (44).

Quantification of HIV-1 RNA and antigen. The amount of HIV-1 RNA in 50 μl of plasma was quantified by Bio Medical Laboratories, Inc. The detection limit of HIV-1 RNA is 1,600 copies/ml. To quantify the amount of cell-free virions in the supernatant of spleen and the BM fluid, the splenic cell suspension and the BM fluid obtained by flushing were centrifuged; the supernatants were filtered through a 0.45-μm-pore-size filter and then ultracentrifuged at 30,000 rpm for 1 h at 4°C by using a TL-100 instrument (Beckman). The pellets were resuspended with phosphate-buffered saline, and the amount of HIV-1 Gag proteins was quantified using an HIV-1 p24 antigen ELISA kit (ZetroMetrix).

Flow cytometry, hematocytometry, and immunostaining. Flow cytometry was performed with a FACSCanto II and a FACSCalibur (BD Biosciences) as previously described (44, 52, 54, 55), and the obtained data were analyzed with CellQuest software (BD Biosciences) and FlowJo software (Tree Star, Inc.). For flow cytometry analysis, the following antibodies were used: fluorescein isothiocyanate (FITC)-conjugated rat anti-HIV-1 p24 monoclonal antibody (clone 2C2, kindly provided by Yuetsu Tanaka) (45), phycoerythrin (PE)-conjugated anti-CD45 antibody (HI30; Biolegend) and anti-SLAMF6 antibody (clone 292811; R&D Systems), allophycocyanin (APC)-conjugated anti-BST2 antibody (RS38E; Biolegend) and anti-CD4 antibody (RPA-T4; Biolegend), PE-Cy7-conjugated anti-CD4 antibody (RPA-T4; Biolegend), APC-Cy7-conjugated anti-CD3 antibody (HIT3a; Biolegend) and anti-CD45 antibody (HI30; Biolegend), peridinin chlorophyll protein (PerCP)-Cy5.5-conjugated anti-CD45RA antibody (HI100; Biolegend), and AmCyan-conjugated anti-CD8 antibody (DK25; Dako). For the costaining of CD4, BST2, SLAMF6, and Gag, surface CD4, BST2, and SLAMF6 were stained prior to fixation. Then, the cells were fixed and permeabilized using a Cytofix/Cytoperm solution (BD biosciences), and intracellular Gag proteins were subsequently stained. Hematocytometry was performed with a Celltac a MEK-6450 (Nihon Kohden, Co.) as previously described (54). Immunostaining was performed with a Leica TCS SP2 AOBS confocal laser microscope (Leica Microsystems) as previously described (44, 54). The obtained pictures were assessed by using ImageJ software (http://rsbweb.nih.gov/ij/). For immunostaining analysis, mouse anti-HIV-1 p24 monoclonal antibody (Kal-1; Dako) and Alexa Fluor 594-conjugated goat anti-mouse IgG antibody (Molecular probes) were used. Nuclei were stained with Hoechst 33342 (Molecular Probes).

PCR analyses. DNA was extracted from the splenic MNCs at 21 days postinfection (dpi) by a urea-lysis method as previously described (25). PCR was performed by using *rTaq* DNA polymerase (TaKaRa) according to the manufacturer's protocol, and the following primers were used: *gag* forward (bases 1484 to 1503), 5′-GGG GAA GTG ACA TAG CAG GA-3′; *gag* reverse (bases 1746 to 1765), 5′-CAT TTT GGA CCA GCA AGG TT-3′; *vpu* forward 1st (bases 5712 to 5731), 5′-GAT ACT TGG GCA GGA GTG GA-3′; *vpu* reverse 1st (bases 6222 to 6241), 5′-CCT GAT CCC CTT CAC TTT CA-3′; *vpu* forward 2nd (bases 5926 to 5945), 5′-TGC CAA GTT TGC TTC ACA AG-3′; *vpu* reverse 2nd (bases 6205 to 6224), 5′-TCA TTG CCA CTG TCT TCT GC-3′; *ACTB* forward, 5′-TCA CCC ACA CTG TGC CCA TCT ACG A-3′; *ACTB* reverse, 5′-CAG CGG AAC CGC TCA TTG CCA ATG G-3′.

Statistical and mathematical analyses. Data were expressed as averages with standard errors of the means (SEMs). Statistical differences were determined by Student's *t* test, Welch's *t* test, or the log rank test. To

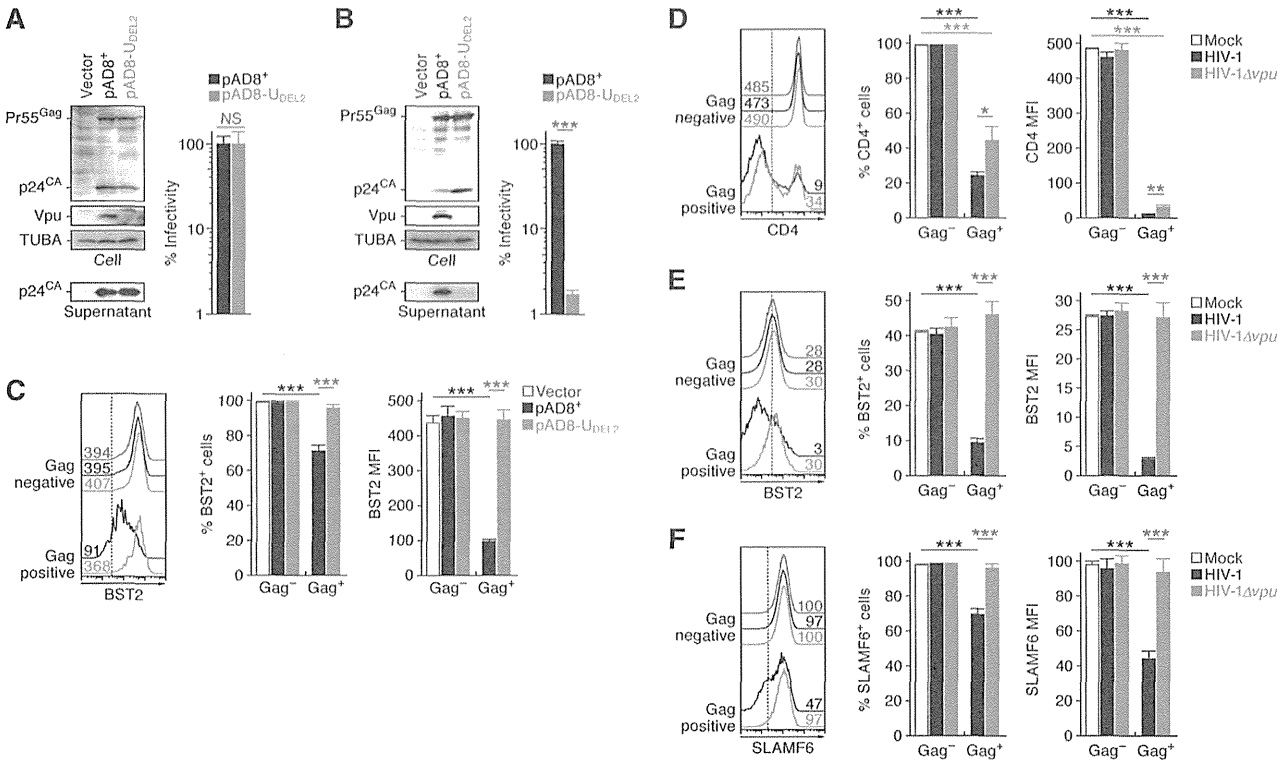

FIG 1 Dynamics of WT and *vpu*-deficient HIV-1 infection in cultured cells. (A to C) HIV-1 release and downregulation of surface BST2. One microgram of pAD8$^+$ (WT HIV-1-producing plasmid) or pAD8-U_{DEL2} (*vpu*-deficient HIV-1-producing plasmid) was transfected into 293T or HeLa cells, respectively. The expression levels of Gag ($Pr55^{Gag}$) and Vpu, the amount of virions retained in the cells ($p24^{CA}$ in the cells), and the amount of released virion ($p24^{CA}$ in the supernatant) in the transfected 293T cells (A) and HeLa cells (B) were determined by Western blotting (left panels). The input of cell lysate was standardized to α-tubulin (TUBA), and representative results are shown. In TZM-bl assays titers of the viruses released from the transfected 293T cells and HeLa cells were determined. The infectivity is shown as the percentage of the value of WT HIV-1. (C) The surface expression level of BST2 on the transfected HeLa cells at 48 h posttransfection was assessed by flow cytometry. The HeLa cells transfected with pAD8$^+$, pAD8-U_{DEL2}, and pUC19 (parental plasmid; Vector) were classified into virus-producing (Gag-positive) or non-virus-producing (Gag-negative) populations by using an antibody against HIV-1 p24 antigen. Representative histograms (left), the percentage of BST2-positive cells (middle), and the MFI of BST2 (right) are shown. In the left panel, the numbers on each histogram indicate the MFI values, and the vertical broken lines indicate the thresholds for the gating of positive cells based on the result from the isotype control. The assay was performed in quadruplicate. (D to F) Primary human CD4$^+$ T cells were prepared as described in Materials and Methods and infected with WT and *vpu*-deficient HIV-1 at an MOI of 0.1. At 7 dpi, the cells were harvested and used for flow cytometry. The cells were classified into infected (Gag-positive) or uninfected (Gag-negative) populations by using an anti-p24 antibody. Representative histograms (left), the positive percentages (middle), and the MFIs (right) of CD4, BST2, and SLAMF6 in each population are shown. In the left panels, the numbers on each histogram indicate the MFI values, and the vertical broken lines indicate the thresholds for the gating of positive cells based on the result from isotype controls. The assay was performed in triplicate. The statistic difference is determined by a Student's *t* test. Statistically significant differences are shown as follows: *, $P < 0.05$; **, $P < 0.01$; ***, $P < 0.001$. Error bars represent SEMs. NS, no statistical significance.

determine a statistically significant correlation (see Fig. 4C), the Pearson correlation coefficient (*r*) was applied. To estimate the 50% infectious dose (ID_{50}) for NOG-hCD34 mice, nonlinear regression analyses (39, 43) were performed by using Mathematica, version 8, software (Wolfram Research).

The GenBank (http://www.ncbi.nlm.nih.gov/GenBank/index.html) accession numbers for the genes and virus mentioned in the text are as follows: for *BST2*, NM_004335.2; for *CD4*, NM_000616.4, for *ACTB*, NM_001101.3; and for HIV-1 strain AD8, AF004394.1.

RESULTS

Dynamics of *vpu*-deficient HIV-1 infection in cultured cells. To assess the impact of HIV-1 Vpu on virus replication, we first confirmed the ability of Vpu, derived from a CCR5-tropic HIV-1 strain AD8, to downregulate BST2 in 293T and HeLa cells. These cell lines were transfected with a plasmid carrying WT HIV-1 strain AD8, pAD8$^+$ (66), or a *vpu*-deficient derivative of AD8, pAD8-U_{DEL2} (62, 63). As previously reported (42, 56, 67), in 293T cells, which do not express endogenous BST2, the absence of *vpu* did not affect the expression level of Gag precursor ($Pr55^{Gag}$), the amount of produced virions, or the infectivity of the released virions (Fig. 1A). On the other hand, in HeLa cells, which endogenously express BST2, the yield of *vpu*-deficient virions released was 60-fold lower than that of WT released virions although the expression level of $Pr55^{Gag}$ was comparable (Fig. 1B). We also found that the surface expression of BST2 on WT HIV-1-producing (i.e., positive for HIV-1 Gag protein) but not *vpu*-deficient HIV-1-producing HeLa cells was significantly and severely downregulated (Fig. 1C). In line with previous reports (42, 56, 67), our results suggest that the Vpu protein encoded by strain AD8 potently downregulates cell surface BST2 and antagonizes its function to enhance the release of nascent virions.

Based on previous reports (8, 26, 31, 64), Vpu is known to

downregulate BST2, CD4, and SLAMF6 from the surface of infected cells. To confirm that the Vpu protein encoded by strain AD8 is able to exert these effects, primary human $CD4^+$ T cells were infected with WT and *vpu*-deficient HIV-1. As shown in Fig. 1D to 1F, we observed that CD4, BST2, and SLAMF6 were significantly downregulated from the surface of WT HIV-1-infected but not of HIV-1Δ*vpu*-infected cells. Because it is well known that CD4 can be downregulated by not only Vpu but also HIV-1 Env and Nef (31), the decrease in CD4 on the surface of HIV-1Δ*vpu*-infected cells is most likely due to the effect of these proteins. Taken together, these findings strongly suggest that the Vpu protein encoded by strain AD8 has the potential to downregulate the reported three molecules *in vitro*.

Dynamics of *vpu*-deficient HIV-1 infection in humanized mice. In order to investigate the role of Vpu in HIV-1 expansion *in vivo*, three different doses (3,000, 30,000, and 300,000 $TCID_{50}$) of WT or *vpu*-deficient HIV-1 (strain AD8) were intraperitoneally inoculated into humanized mice. Seventy humanized mice, which were reconstituted with $CD34^+$ hematopoietic stem cells from eight individual donors, were used for this study (Table 1). Out of the 70 humanized mice, 32 mice were infected with WT HIV-1 (3,000 $TCID_{50}$, $n = 6$; 30,000 $TCID_{50}$, $n = 5$; and 300,000 $TCID_{50}$, $n = 21$), 31 mice were infected with *vpu*-deficient HIV-1 (3,000 $TCID_{50}$, $n = 6$; 30,000 $TCID_{50}$, $n = 5$; and 300,000 $TCID_{50}$, $n = 20$), and the remaining 7 mice were used for mock infection. The amounts of viral RNA in plasma were assessed at 3, 7, 14, and 21 dpi. As shown in Fig. 2A, humanized mice were more efficiently infected with WT HIV-1 than *vpu*-deficient HIV-1 (300,000 $TCID_{50}$, $P = 0.013$ by the log rank test). In addition, nonlinear regression analyses revealed that the ID_{50} in NOG-hCD34 mice for WT HIV-1 was 2.3-fold lower than that for *vpu*-deficient HIV-1 (for WT HIV-1, 1 ID_{50} is 1,343 $TCID_{50}$; $r = 0.999$, $P = 1.6 \times 10^{-7}$; for HIV-1Δ*vpu*, 1 ID_{50} is 3,046 $TCID_{50}$; $r = 0.990$, $P = 0.019$). These findings suggest that our humanized mice are more susceptible to WT HIV-1 than *vpu*-deficient HIV-1. Moreover, the amount of viral RNA in the plasma of WT HIV-1-infected mice increased more rapidly (Fig. 2B) and was 8.5-fold higher at 7 dpi than in HIV-1Δ*vpu*-infected mice (300,000 $TCID_{50}$; $P = 0.049$). Taken together, these findings suggest that WT HIV-1 propagates more rapidly and efficiently in humanized mice than *vpu*-deficient HIV-1 during the initial phase of infection.

We next analyzed the numbers of total $CD4^+$ T cells, $CD45RA^+$ naive $CD4^+$ T cells, and $CD45RA^-$ memory $CD4^+$ T cells in the PB of infected mice. As shown in Fig. 2C to E, virus infection at lower doses (3,000 and 30,000 $TCID_{50}$) did not affect the numbers of peripheral $CD4^+$ T cells. On the other hand, at a high infection dose (300,000 $TCID_{50}$) in WT HIV-1-infected mice, the number of total $CD4^+$ T cells, naive T (Tn) cells, and memory T (Tm) cells decreased by 4.0-fold, 2.4-fold, and 4.8-fold, respectively (Fig. 2C to E). Interestingly, this observed decrease in analyzed T cells in WT HIV-1-infected mice at 14 and 21 dpi was indistinguishable from that in HIV-1Δ*vpu*-infected mice (Fig. 2C to E). Similarly, we observed that the percentages of $CD4^+$ T cells, particularly Tm cells, in spleen and BM of both WT and *vpu*-deficient HIV-1-infected mice at 7 and 21 dpi was significantly lower than those of uninfected mice and that the reduced levels of total $CD4^+$ T cells and Tm cells in WT HIV-1-infected mice were comparable to those in *vpu*-deficient HIV-1-infected mice (Fig. 2F). Taken together, these results suggest that the cytotoxicity induced by WT HIV-1 was similar to that of *vpu*-deficient HIV-1 in humanized mice.

Reduced production of *vpu*-deficient HIV-1 particles in the spleen of humanized mice at 7 dpi. To exclude the possibility of *vpu* reversion in HIV-1Δ*vpu*-infected mice, we performed PCR targeting the *vpu*-coding region and confirmed that the 81-bp deletion in *vpu* was maintained even at 21 dpi (Fig. 3A). This result indicates that *vpu* reversion did not occur in HIV-1Δ*vpu*-infected mice. We then assessed the proportion of HIV-1-infected cells (i.e., Gag-positive cells) in WT and *vpu*-deficient HIV-1-infected mice. As previously reported (44), we found that the majority of HIV-1-infected cells in the spleen of WT HIV-1-infected humanized mice were $CD3^+$ $CD45RA^-$ Tm cells (Fig. 3B and C). Infected splenic cells of HIV-1 Δ*vpu*-infected mice also consisted of Tm cells, and the level was equal to that of WT HIV-1-infected mice (Fig. 3B and C). These results suggest that *vpu* deficiency did not affect the preference of target cells.

In order to investigate the level of HIV-1 replication in organs, we collected PB/plasma, spleen, and BM of mice infected with 300,000 $TCID_{50}$ at 7 and 21 dpi and analyzed the specimens by HIV-1 p24 ELISA and flow cytometry. As shown in Fig. 4A, the amounts of cell-free virions in the spleen of both WT and *vpu*-deficient HIV-1-infected mice were predominantly higher than those in plasma and BM, suggesting that the spleen is a major site for viral replication. At 21 dpi, when the level of viral RNA in the plasma of WT HIV-1-infected mice was similar to that of HIV-1Δ*vpu*-infected mice (Fig. 2B, right panel), the amounts of viral particles (Fig. 4A) and the percentages of HIV-1-infected cells (Fig. 4B) in all tissues we analyzed in both groups of mice were comparable. On the other hand, at 7 dpi when the amount of viral RNA in the plasma of WT HIV-1-infected mice was significantly higher than that of HIV-1Δ*vpu*-infected mice (Fig. 2B, right panel), the percentage of Gag-positive cells in the spleen of WT HIV-1-infected mice was 2.8-fold higher than that of HIV-1Δ*vpu*-infected mice (Fig. 4B). It was of interest that the amount of cell-free viral particles in the spleen of WT HIV-1-infected mice at 7 dpi was profoundly (38.2-fold) higher than that of HIV-1Δ*vpu*-infected mice (Fig. 4A). Furthermore, in the spleen of WT HIV-1-infected mice at 7 dpi, the amount of the cell-free virions significantly correlated with the percentage of infected cells, whereas no correlation in the spleen of HIV-1Δ*vpu*-infected mice was observed (WT HIV-1, $r = 0.877$ and $P = 0.00085$; HIV-1Δ*vpu*, $r = 0.344$ and $P = 0.37$) (Fig. 4C). These findings indicate that Vpu might enhance the expression of viral proteins, which lead to a robust production of viral particles. To address this possibility, the mean fluorescent intensity (MFI) of HIV-1 Gag in WT and *vpu*-deficient HIV-1-infected splenic cells was measured. Because the reagents for flow cytometry preferentially permeabilize plasma membranes, the anti-p24 antibody we used had access to the Gag proteins in the cytoplasm (i.e., $Pr55^{Gag}$), which indicates that the MFI value of Gag can reflect the level of expressed $Pr55^{Gag}$ in proteins in infected cells. However, as shown in Fig. 4D, the levels of Gag MFI in WT and *vpu*-deficient HIV-1-infected splenic cells were equal. This result suggests that Vpu does not affect the expression of viral proteins leading to the augmentation of virion production.

Downregulation of the surface expression levels of Vpu-associated cellular proteins on infected cells in humanized mice at 7 dpi. As shown in Fig. 1D to F, we demonstrated that Vpu downregulates CD4, BST2, and SLAMF6 from the surfaces of *vpu*-pro-

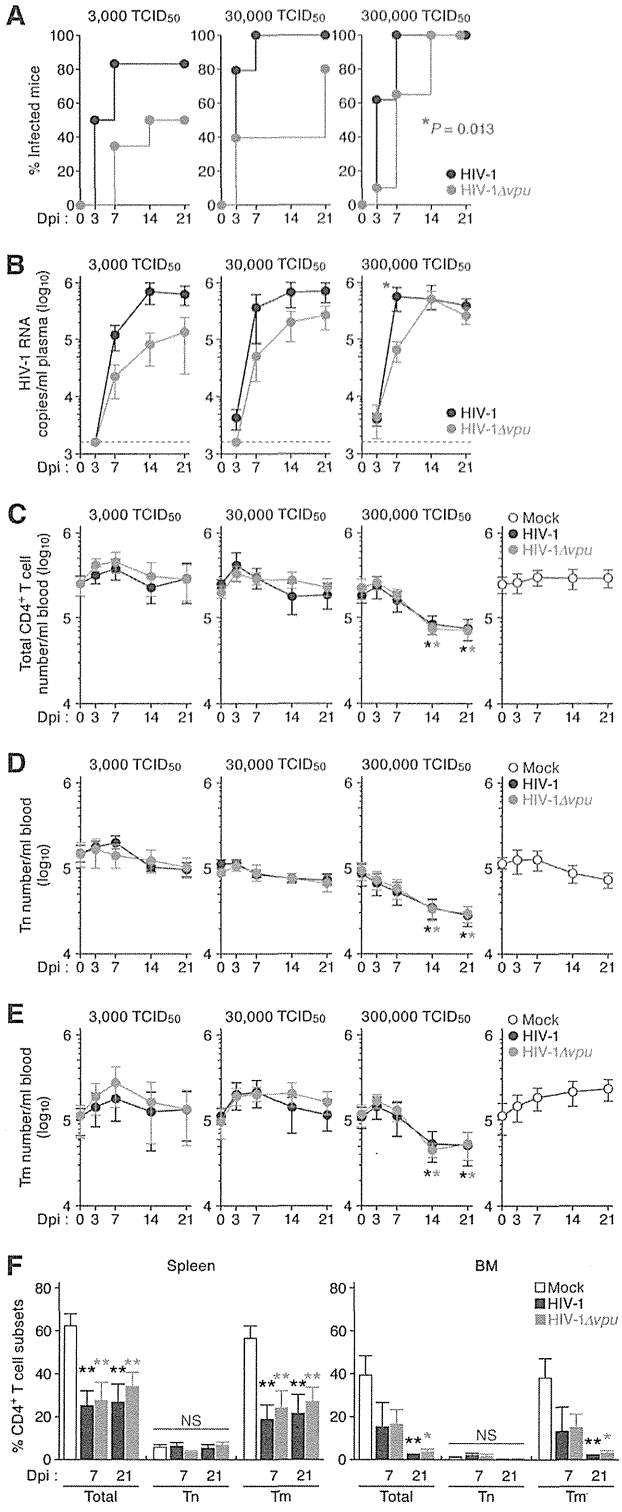

FIG 2 Dynamics of WT and *vpu*-deficient HIV-1 infection in humanized mice. (A and B) Expansion of WT and *vpu*-deficient HIV-1 in humanized mice. WT HIV-1 (3,000 $TCID_{50}$, $n = 6$; 30,000 $TCID_{50}$, $n = 5$; and 300,000 $TCID_{50}$, $n = 21$) and *vpu*-deficient HIV-1 (3,000 $TCID_{50}$, $n = 6$; 30,000 $TCID_{50}$, $n = 5$, and 300,000 $TCID_{50}$, $n = 20$) were inoculated into humanized mice aged between 12 and 17 weeks old, and the amount of viral RNA in plasma was quantified at 3, 7, 14, and 21 dpi. (A) Frequency of infection in mice. The percentage of infected mice in which viral RNA in plasma was detected at each time point is presented as Kaplan-Meier curves. (B) Viral load in infected humanized mice. The horizontal broken line indicates the detection limit of the assay (1,600 copies/ml). (C to E) Cytopathic effect of WT and *vpu*-deficient HIV-1 in the PB of humanized mice. The numbers of total $CD4^+$ T cells ($CD45^+$ $CD3^+$ $CD4^+$ cells; C), Tn cells ($CD45^+$ $CD3^+$ $CD4^+$ $CD45RA^+$ cells; D), and Tm cells ($CD45^+$ $CD3^+$ $CD4^+$ $CD45RA^-$ cells; E) in the PB of WT HIV-1-infected mice (3,000 $TCID_{50}$, $n = 6$; 30,000 $TCID_{50}$, $n = 5$, and 300,000 $TCID_{50}$, $n = 11$), *vpu*-deficient HIV-1-infected mice (3,000 $TCID_{50}$, $n = 6$; 30,000 $TCID_{50}$, $n = 5$, and 300,000 $TCID_{50}$, $n = 11$), and mock-infected mice ($n = 7$) were routinely analyzed by flow cytometry and hematocytometry. (F) Cytopathic effect of WT and *vpu*-deficient HIV-1 in the lymphoid tissues of humanized mice. The percentages of total $CD4^+$ T cells, Tn cells, and Tm cells in the spleen (left) and the BM (right) of WT HIV-1-infected mice (300,000 $TCID_{50}$, $n = 7$) and *vpu*-deficient HIV-1-infected mice (300,000 $TCID_{50}$, $n = 7$), and mock-infected mice (21 dpi, $n = 6$) were analyzed by flow cytometry. In panel A, statistical difference was determined by a log rank test. In panel B, statistical difference between WT HIV-1 versus *vpu*-deficient HIV-1 was determined by Welch's *t* test. In panels C to F, statistical difference between mock-infected versus WT HIV-1- or *vpu*-deficient HIV-1-infected mice was determined by Welch's *t* test. Statistically significant differences are shown as follows: *, $P < 0.05$; **, $P < 0.01$; ***, $P < 0.001$. Error bars represent SEMs. NS, no statistical significance.

ficient HIV-1-infected cells *in vitro*. To address whether the potential of Vpu to downregulate these three molecules is associated with the decrease of cell-free virions in HIV-1Δ*vpu*-infected mice (Fig. 4A), we focused on the surface expression levels of CD4, BST2, and SLAMF6 on infected cells (i.e., Gag-positive cells). Since the difference in the levels of plasma viral load (Fig. 2B, right panel) and splenic cell-free virions (Fig. 4A) between WT HIV-1-infected mice and HIV-1Δ*vpu*-infected mice is most significant at the higher infection dose (300,000 $TCID_{50}$) at 7 dpi, we used the splenic specimen of mice infected under these conditions. Because the majority of infected cells were Tm cells (Fig. 3B and C), we analyzed the surface levels of these three proteins on Tm ($CD3^+$ $CD8^-$ $CD45RA^-$) cells by flow cytometry. As observed in *in vitro* experiments (Fig. 1D), we detected a significant downregulation of surface CD4 in both WT and *vpu*-deficient HIV-1-infected cells (Fig. 5A). Nevertheless, we also found that both the percentage and the MFI of surface CD4 in Gag-positive cells in WT HIV-1-infected mice were significantly lower than those in HIV-1Δ*vpu*-infected mice (Fig. 5A), which suggests that Vpu potently downregulates CD4 even *in vivo*. Interestingly, BST2 expressed on WT but not on *vpu*-deficient HIV-1-infected cells was significantly downregulated (Fig. 5B). On the other hand, Vpu-dependent downregulation of SLAMF6 on infected cells was not observed in infected humanized mice (Fig. 5C). Taken together, these results suggest that Vpu downregulates CD4 and BST2 from the surface of infected cells, which leads to the impairment of the release of nascent virions.

In order to investigate the dynamics of CD4 and BST2 in depth, we classified infected and uninfected cells into four types: $CD4^+$ $BST2^+$, $CD4^+$ $BST2^-$, $CD4^-$ $BST2^+$, and $CD4^-$ $BST2^-$. In Gag-negative Tm cells ($CD3^+$ $CD8^-$ $CD45RA^-$ Gag^-) of mock-infected, WT HIV-1-infected, and HIV-1Δ*vpu*-infected mice, most of the cells expressed CD4, while approximately 60% of the cells were positive for BST2 (Fig. 6A to D). On the other hand, in Gag-positive Tm cells ($CD3^+$ $CD8^-$ $CD45RA^-$ Gag^+) of WT HIV-1-infected mice, we detected a significant level of the cells negative for both CD4 and BST2, and the percentage of $CD4^-$ $BST2^-$ cells was significantly higher than that of $CD4^-$ $BST2^+$ cells

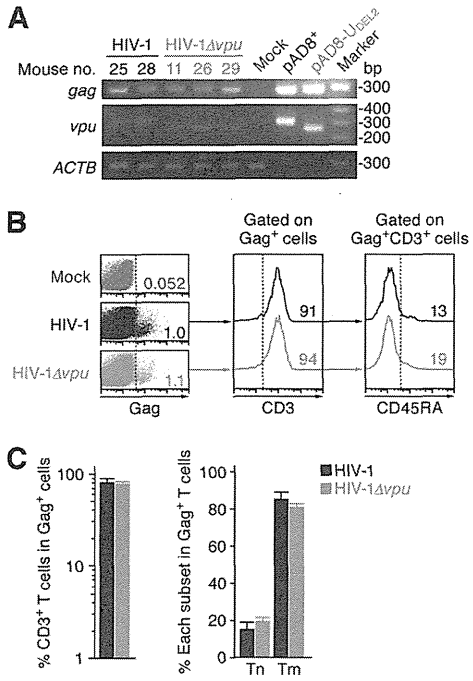

FIG 3 Characteristics of infected cells in humanized mice. (A) PCR analysis of proviral DNA. The regions of *gag* and *vpu* in HIV-1 DNA in the spleen of two WT HIV-1-infected mice, three *vpu*-deficient HIV-1-infected mice, and a mock-infected mouse at 21 dpi were analyzed by PCR. The mouse numbers correspond to those in Table 1. A representative result is shown. As the positive controls for *gag* and *vpu*, a WT HIV-1 plasmid (pAD8$^+$) and *vpu*-deficient HIV-1 plasmid (pAD8-U_{DEL2}) were used. Note that the band size of *vpu* in *vpu*-deficient HIV-1-infected mice is smaller than that in WT HIV-1-infected mice because of the 81-bp deletion with frameshift (see Materials and Methods for detail). ACTB (β-actin) was used as the internal control of the assay. (B and C) Characterization of infected cells. Human MNCs in the spleen of WT HIV-1-infected mice, *vpu*-deficient HIV-1-infected mice, and mock-infected mice were analyzed by flow cytometry. Representative dot plots and histograms are shown (B). The numbers in dot plots and histograms indicate the percentages of positive cells in each parental population, and the vertical broken lines indicate the threshold for the gating of positive cells based on the result from the isotype controls. (C) The percentages of CD3$^+$ T cells in Gag-positive cells (left) and the percentages of Tn cells (CD45RA$^+$) and Tm cells (CD45RA$^-$) in infected T cells (Gag$^+$ CD3$^+$ CD8$^-$cells, right) in the spleen of WT HIV-1-infected mice (n = 7) and *vpu*-deficient HIV-1-infected mice (n = 8) are shown.

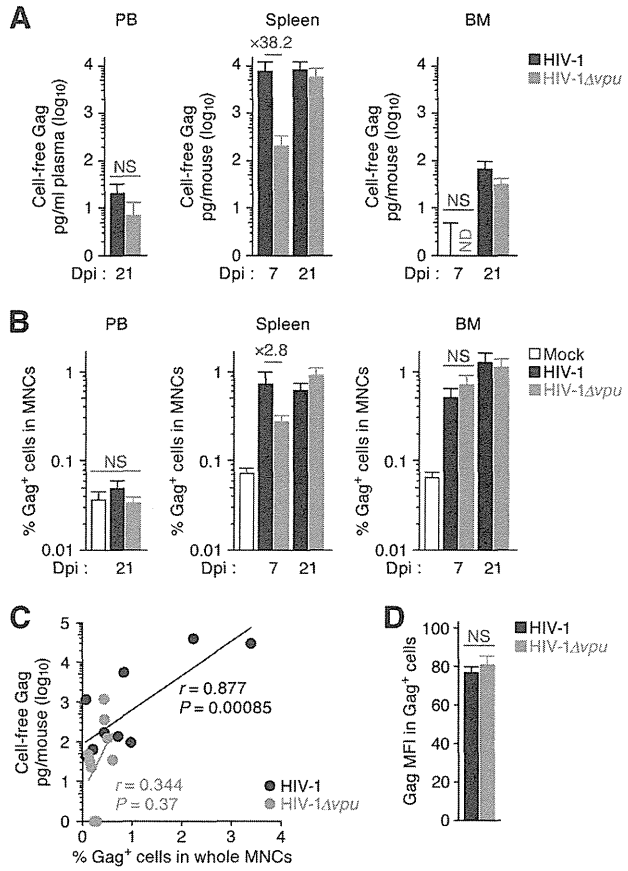

FIG 4 Viral dissemination in the PB and lymphoid organs of humanized mice. (A) Cell-free virions in the PB and lymphoid organs of infected mice. The amounts of cell-free virus in the plasma (left), the supernatant of splenic suspension (middle), and the BM fluid (right) of WT HIV-1-infected mice (300,000 $TCID_{50}$, 7 and 21 dpi; n = 7) and *vpu*-deficient HIV-1-infected mice (300,000 $TCID_{50}$, 7 and 21 dpi; n = 8) were quantified by p24 ELISA. (B) The percentage of HIV-1 Gag-positive cells in the PB (left), the spleen (middle), and the BM (right) of WT HIV-1-infected mice (300,000 $TCID_{50}$, 7 and 21 dpi; n = 7), *vpu*-deficient HIV-1-infected mice (300,000 $TCID_{50}$, 7 and 21 dpi; n = 8), and mock-infected mice (21 dpi; n = 7) were analyzed by flow cytometry. (C) Correlation of the amount of cell-free virions and the percentage of infected cells. The results of the percentage of Gag-positive cells in spleen at 7 dpi (x axis) and the amount of cell-free Gag proteins in splenic fluid at 7 dpi (y axis) from WT HIV-1-infected mice (300,000 $TCID_{50}$; n = 10) and *vpu*-deficient HIV-1-infected mice (300,000 $TCID_{50}$; n = 9) are plotted. The lines represent exponential approximation. The Pearson correlation coefficient (r) was adopted to determine statistically significant correlation between each value, and a P value of <0.05 was considered statistically significance. (D) The MFIs of Gag ($Pr55^{Gag}$) in Gag-positive cells (right) in the spleen of WT HIV-1-infected mice (300,000 $TCID_{50}$; n = 7) and *vpu*-deficient HIV-1-infected mice (300,000 $TCID_{50}$; n = 7) were analyzed by flow cytometry at 7 dpi. Error bars represent SEMs. ND, not detected; NS, no statistical significance.

(CD4$^-$ BST2$^-$ cells, 36.6% ± 3.8%; CD4$^-$ BST2$^+$ cells, 3.5% ± 1.4%) (Fig. 6B and E). In contrast, in Gag-positive Tm cells of HIV-1Δ*vpu*-infected mice, the percentage of CD4$^-$ BST2$^-$ cells was significantly lower than that of CD4$^-$ BST2$^+$ cells (CD4$^-$ BST2$^-$ cells, 5.3% ± 0.8%; CD4$^-$ BST2$^+$ cells, 14.2% ± 0.9%) (Fig. 6B and E). Furthermore, the percentage of CD4$^-$ BST2$^-$ Tm cells positive for Gag in WT HIV-1-infected mice was significantly higher than that in HIV-1Δ*vpu*-infected mice (Fig. 6E). Taken together, these results suggest that Vpu concomitantly downregulates the cell surface expression of CD4 and BST2 in infected cells.

Modulation of the surface expression levels of Vpu-associated cellular proteins in infected humanized mice at 21 dpi. Although a marked difference in the levels of plasma viral load and cell-free virions in the spleen of WT HIV-1-infected and HIV-1Δ*vpu*-infected mice was observed at 7 dpi, the viral loads became comparable at 21 dpi (Fig. 2B, right panel). To explore the possibility that Vpu loses its ability to downregulate CD4 and BST2 at 21 dpi, we used the splenic specimens at this time point and analyzed the surface levels of CD4, BST2, and SLAMF6 by flow cytometry. In contrast to this hypothesis, we detected significant downregulation of CD4 and BST2 on WT HIV-1-infected Tm cells (Fig. 7A and B). Although a significant downregulation of SLAMF6 was also observed in infected Tm cells, it was independent on Vpu (Fig. 7C). Unexpectedly, we found that BST2 was

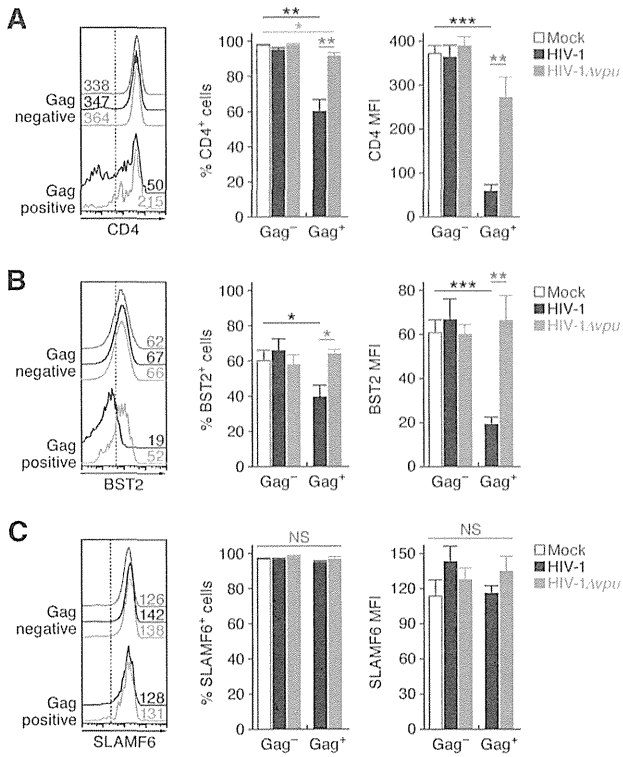

FIG 5 Surface expression profile of CD4, BST2, and SLAMF6 in infected humanized mice at 7 dpi. Tm cells ($CD3^+$ $CD8^-$ $CD45RA^-$) in the spleen of WT HIV-1-infected mice (300,000 $TCID_{50}$; $n = 7$), *vpu*-deficient HIV-1-infected mice (300,000 $TCID_{50}$; $n = 6$), and mock-infected mice ($n = 7$) at 7 dpi were classified into infected (Gag-positive) or uninfected (Gag-negative) populations by using an anti-p24 antibody. Representative histograms (left), the positive percentages (middle), and the MFIs (right) of CD4 (A), BST2 (B), and SLAMF6 (C) in each population are shown. In the left panels, the numbers on each histogram indicate the MFI values, and the vertical broken lines indicate the thresholds for the gating of positive cells based on the result from the isotype controls. The statistical difference is determined by Welch's *t* test. Statistically significant differences are shown as follows: *, $P < 0.05$; **, $P < 0.01$; ***, $P < 0.001$. Error bars represent SEMs. NS, no statistical significance.

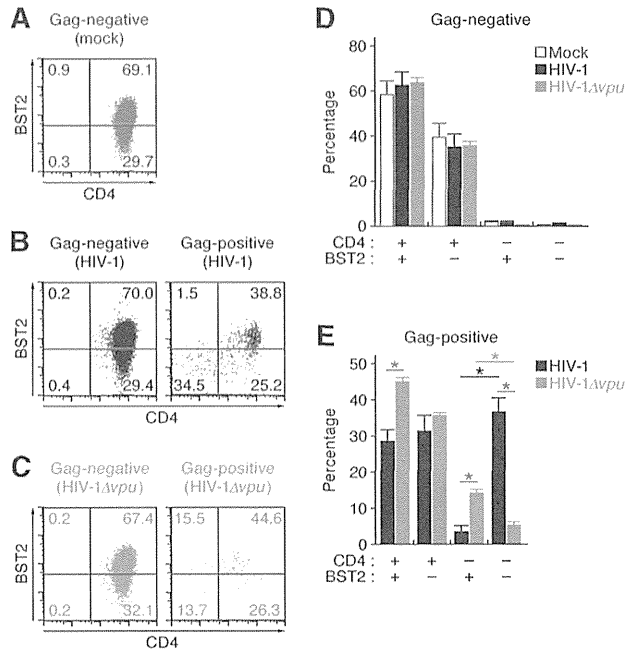

FIG 6 Codownregulation of CD4 and BST2 from the surface of WT HIV-1-infected cells. Surface expression levels of CD4 and BST2 on the surface of Gag-positive Tm cells ($CD3^+$ $CD8^-$ $CD45RA^-$ Gag^+) or Gag-negative Tm cells ($CD3^+$ $CD8^-$ $CD45RA^-$ Gag^-) in the spleen of WT HIV-1-infected mice (300,000 $TCID_{50}$; $n = 6$), *vpu*-deficient HIV-1-infected mice (300,000 $TCID_{50}$; $n = 5$), and mock-infected mice ($n = 7$) at 7 dpi were analyzed by flow cytometry. Representative dot plots (A to C) and the summarized results (D and E) are shown. In panels A to C, the numbers indicate the percentages of the cells in the respective quadrant. The statistical difference is determined by Welch's *t* test (*, $P < 0.05$). Error bars represent SEMs.

upregulated on Gag-negative Tm cells of HIV-1Δ*vpu*-infected mice (Fig. 7B). Since the upregulation of BST2 was observed in Gag-negative Tm cells of not only HIV-1Δ*vpu*-infected mice but also WT HIV-1-infected mice (Fig. 7B), we speculated that this increase was independent of Vpu and is indirectly induced by HIV-1 infection. To address this issue, we analyzed the expression level of BST2 on the other human leukocytes, which were less susceptible or resistant to HIV-1 infection. As shown in Fig. 7D and E, the levels of surface BST2 on Tn cells and $CD8^+$ T cells of WT HIV-1- and HIV-1Δ*vpu*-infected mice were significantly higher than those of mock-infected mice. These findings suggest that CD4 and BST2 were still downregulated by Vpu at 21 dpi, while BST2 is upregulated on uninfected cells in infected mice.

Cell-to-cell contact of infected cells in the spleen of infected mice. To investigate why the viral loads were equal at 21 dpi (Fig. 2B, right panel), we performed immunostaining analysis in the spleen of WT HIV-1- and HIV-1Δ*vpu*-infected mice (Fig. 8A). Interestingly, results (Fig. 8B) revealed that most of the Gag-positive cells were in contact with the other adjunct Gag-positive cell(s) in the spleen of WT HIV-1- and HIV-1Δ*vpu*-infected mice (WT HIV-1, 84.2%; HIV-1Δ*vpu*, 82.4%) (Fig. 8C). These findings suggest that cell-to-cell viral transmission frequently occurs in the spleens of WT HIV-1- and HIV-1Δ*vpu*-infected mice.

The different effects of CD4 and BST2 on cell-free and cell-to-cell HIV-1 infection *in vitro*. To directly demonstrate the potential of CD4 and BST2 to inhibit cell-free and cell-to-cell infections of HIV-1, $pAD8^+$ or pAD8-U_{DEL2} was cotransfected with or without CD4 or BST2 expression plasmids into HEK293 cells in which neither CD4 nor BST2 is endogenously expressed (56). As observed in infected humanized mice (Fig. 5 and 6), ectopically expressed CD4 and BST2 were downregulated in a Vpu-dependent manner (Fig. 9A and B). In addition, in the cells cotransfected with CD4 or BST2 expression plasmids, the percentage of the cells negative for both CD4 and BST2 in $pAD8^+$-transfected cells was significantly higher than percentages in pAD8-U_{DEL2}-transfected and mock-transfected cells (Fig. 9C). These results suggest that CD4 and BST2 were concurrently downregulated by Vpu, reflecting observations in our humanized mouse model (Fig. 6).

We then measured the yield of the released virions in the supernatant and found that the release of *vpu*-deficient HIV-1 was suppressed by CD4 and BST2 (Fig. 9D). Interestingly, the yield of *vpu*-deficient HIV-1 in the supernatant of the cells cotransfected with both CD4 and BST2 expression plasmids was significantly

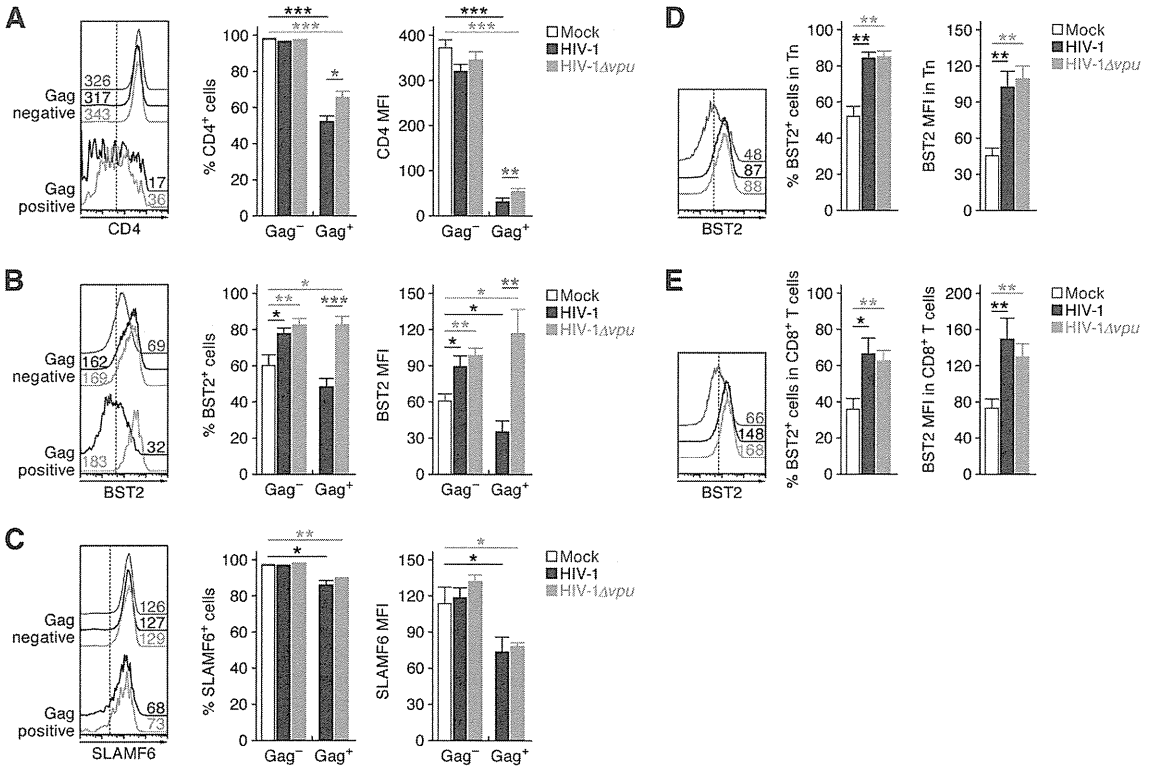

FIG 7 Surface expression profile of CD4, BST2, and SLAMF6 in infected humanized mice at 21 dpi. Tm cells ($CD3^+$ $CD8^-CD45RA^-$; A to C), Tn cells ($CD3^+$ $CD8^-$ $CD45RA^+$; D), and $CD8^+$ T cells ($CD3^+$ $CD8^+$; E) in the spleen of WT HIV-1-infected mice (300,000 $TCID_{50}$; $n = 5$), *vpu*-deficient HIV-1-infected mice (300,000 $TCID_{50}$; $n = 7$), and mock-infected mice ($n = 7$) at 21 dpi were analyzed by flow cytometry. Tm cells were further classified into infected (Gag-positive) or uninfected (Gag-negative) populations by using an anti-p24 antibody. Representative histograms (left), the positive percentages (middle), and the MFIs (right) of CD4 (A), BST2 (B, D, and E), and SLAMF6 (C) in each population are shown. In the left panels, the numbers on the histograms indicate the MFI values, and the vertical broken lines indicate the thresholds for the gating of positive cells based on the result from the isotype controls. The statistical difference is determined by Welch's *t* test. Statistically significant differences are shown as follows: *, $P < 0.05$; **, $P < 0.01$; ***, $P < 0.001$. Error bars represent SEMs. NS, no statistical significance.

lower than that of the cells transfected solely with either CD4 or BST2 expression plasmid alone (Fig. 9D), suggesting that CD4 and BST2 impair the production of nascent virions through distinct manners.

Finally, we quantified the infectious potential of transfected cells by coculturing them with TZM-bl cells. Interestingly, the infectious potential of pAD8-U_{DEL2}-transfected cells was not suppressed by ectopic expression of either CD4 or BST2 either alone or together and was comparable to that of $pAD8^+$-transfected cells (Fig. 9E). Taken together, these findings suggest that CD4

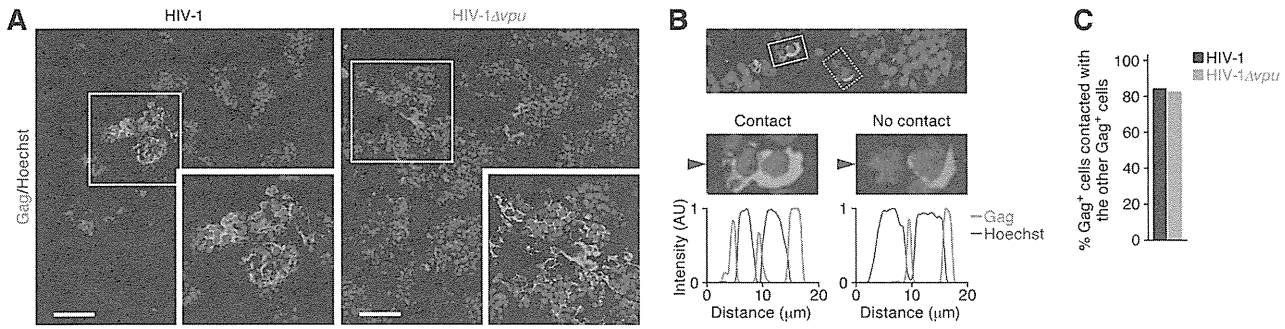

FIG 8 Immunostaining for HIV-1 Gag protein.(A) Representatives of the spleen of WT HIV-1-infected mice (left) and *vpu*-deficient HIV-1-infected mice (right). HIV-1 Gag is shown in red, and nuclei are shown in blue by staining with Hoechst 33342. Boxed areas are enlarged in the bottom right of each panel. Scale bar, 50 μm. (B) A representative of the Gag-positive cell contacted with (solid-line box) or without (broken-line box) the other adjunct Gag-positive cell in spleen is shown (top). The middle panel shows enlargements of the boxed areas. (bottom) The fluorescent intensities of Hoechst (blue) and Gag (red) indicated by arrowheads in the middle panels are shown. AU, arbitrary unit. (C) The percentages of the Gag-positive cells that are contacted with the other adjunct Gag-positive cells in the spleen of WT HIV-1-infected mice ($n = 272$) and *vpu*-deficient HIV-1-infected mice ($n = 448$) are shown.